ACS APPLIED POLYMER MATERIALS

pubs.acs.org/acsapm Review

Photoresponsive Polymer and Polymer Composite Membranes for Gas Separation

Anastasiia Gafiullina, Bradley P. Ladewig, and Jinju Zhang*

Cite This: ACS Appl. Polym. Mater. 2023, 5, 1−30 Read Online

ACCESS | Metrics & More | Article Recommendations

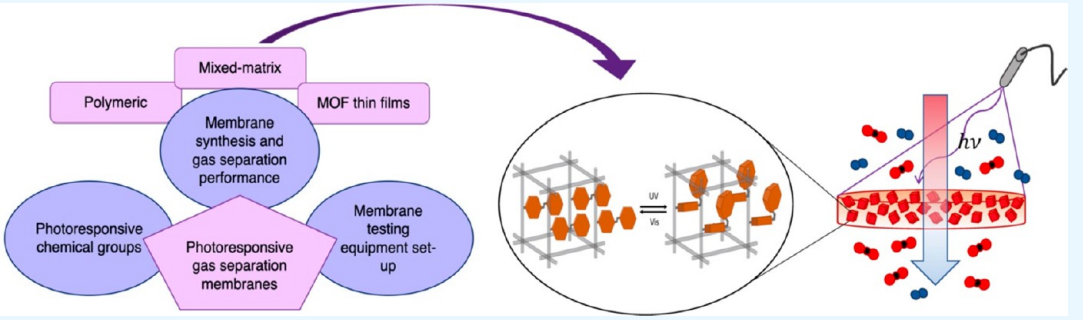

ABSTRACT: Stimuli-responsive materials, referred to as "smart" or "intelligent" materials, have gained significant attention in the separation fields, including gas separation. Among a variety of available stimuli, the use of light as a nondestructive, cost-efficient, chemical-reagent-free stimulus with a relatively fast response is very promising. Herein, we summarize and highlight the approaches applied for the synthesis of photoresponsive organic polymeric membranes, inorganic metal−organic framework thin films, and inorganic−organic mixed-matrix membranes. We discuss the application of these materials for gas separation and provide selected state-of-the-art examples from recently conducted studies. Additionally, the photoresponsive gas separation membrane testing cell plays a crucial role in evaluating and comparing the performance of photoresponsive membranes in the gas separation process. Therefore, we review the development of photoresponsive gas separation membrane testing cells along with the ascribed drawbacks and limitations. A third generation testing system designed to highlight test accuracy is proposed and discussed.

KEYWORDS: *Photoresponsive molecules, Gas separation membranes, Photoresponsive metal−organic frameworks, Photoresponsive mechanisms, Gas separation equipment setup*

1. INTRODUCTION

With the development of science and technology, humanity has become able to face more and more complex issues in various fields: healthcare, technology, the environment, and others. One of the strategies to address problems is to look for similarities in nature to find solutions. Inspired by living systems, it becomes possible to develop functional materials that inherit sensing mechanisms. Such mechanisms provide the ability to respond to changes in environmental conditions by changing the structure and function of the materials.[1−3] Stimuli that respond are numerous and can be placed into two groups based on (1) direct stimuli such as pH, salt ion concentrations, and the redox state or more specific chemical and biological cues—where a material needs to come into direct contact with a stimulation agent (a molecule or an ion); (2) indirect stimuli such as temperature, ultrasound, electric and magnetic fields, or light irradiation, where changes in the material properties are triggered by external stimuli.

The choice of a stimulus and, hence, the related a stimuli-responsive moiety to be added is mainly defined from a material's ultimate application as some types of stimuli may not suit the chosen environment. For example, biomedical applications may find pH, temperature, and biocue responsive biocompatible polymers the most useful as they may fit specific conditions in environments in human bodies. At the same time, in separation technology, the preferences are toward materials that are triggered by physical phenomena, as there is no introduction of additional chemicals into the system. For gas separation membranes, the adoption of the moieties that respond to light seems to be a reasonable choice as changes in a light wavelength only affect the membrane with the introduced functionalities and not the mixture gas properties or experimental setups. Moreover, material response to light

Received: January 14, 2022
Accepted: September 14, 2022
Published: December 7, 2022

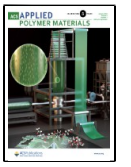

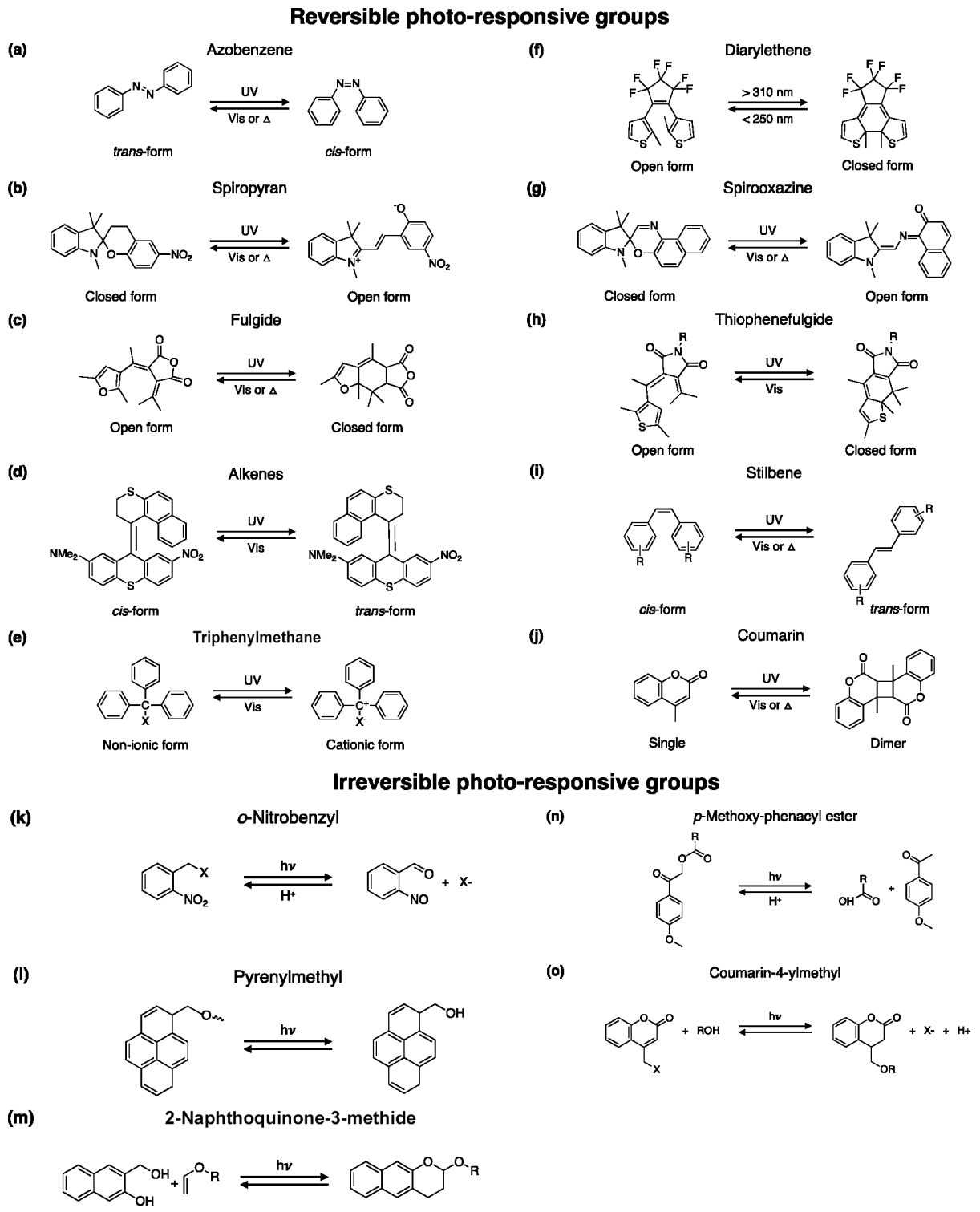

Figure 1. Schematic illustration of photoinduced isomerization in reversible and photochemical reactions in irreversible chromophores: (a) azobenzene, (b) spiropyran, (c) fulgide, (d) alkene, (e) triphenylmethane, (f) diarylethene, (g) spirooxazine, (h) thiophenefulgide, (i) stilbene, (j) coumarin, (k) *o*-nitrobenzyl, (l) pyrenylmethyl, (m) 2-naphthoquinone-3-methide, (n) *p*-methoxyphenacyl ester, (o) coumarin-4-ylmethyl.

irradiation is much faster than the reaction to pH or temperature exposure, whereas the membrane does not experience harsh conditions associated with the previously mentioned stimuli.[4]

Gas separation is an emerging field. Among the industrially applied techniques, membrane separation has demonstrated the capability of reducing an enormous amount of energy input, which is associated with a large part of the operational costs, and it links sustainability of the process. It should be noted that developing a high-efficiency separation technology and designing high-performance membrane materials are the core issues of membrane-based separation technology. Depending on the material of the membrane, gas separation membranes can be divided into three main categories: organic

https://doi.org/10.1021/acsapm.2c00090
ACS Appl. Polym. Mater. 2023, 5, 1−30

(made from polymeric materials), inorganic porous (metal−organic frameworks (MOFs), zeolites, ceramic), and inorganic−organic composite (inorganic fillers mixed within polymeric matrix) membranes.

Photoresponsive gas separation membranes have chemical groups that undergo specific changes in molecular size and geometry upon irradiation of light at different wavelengths. The photoinduced structural changes in molecular photoswitches include planar to orthogonal transformations, opening/closing of a cyclic ring in a molecule, or molecule dimerization. The structural transformations are usually accompanied by alterations in dipole moment, polarity, and hydrophilicity of the photoresponsive molecules. All of these changes would influence the gas transport behavior of the membrane: structural transformations mainly impact the permeance of gases through the membrane, whereas chemical interactions between the introduced photoresponsive groups and gases in a gas mixture affect membrane selectivity by inhibiting transportation of some gases.

In this review, the synthesis and application of photoresponsive membranes are summarized; moreover, the related testing approaches are highlighted. To start with, possible photoresponsive chemical groups and their light-induced transformations are briefly described. In the next section, the practiced synthetic approaches for photoresponsive membrane fabrication are given followed by a discussion of the results of recent studies to illustrate changes in membrane properties due to the light irradiation and the employed photoresponsive and separation mechanisms. Further, a typical photoresponsive gas separation membrane testing setup is discussed with state-of-the-art examples, and their advantages and disadvantages are highlighted. In particular, a remarkable design of the photoresponsive membrane testing setup is first proposed that ensures more accurate temperature control and provides stable light intensity.

2. PHOTORESPONSIVE CHEMICAL GROUPS

When irradiated by light of a specific wavelength, chromophore species can undergo either reversible or irreversible conversion (photoisomerization) between isomeric forms. The ability for photoisomerization comes from the sensitivity of polymers toward the surrounding environment (entropy and, hence, surface energy of the system) provoking reorientations on the material surface appearing as changes in polymer conformation along the backbones, side chains, segments, or end groups.[5] These reorientations change polymer properties such as polarity, chirality, molecular alignment, coordinative interactions, hydrophilicity, solubility, adsorption, and electrical and optical properties. On a larger scale, it displays itself as changes in membrane surface charge, roughness and wettability, permeability, and selectivity.[6−8]

Examples of irreversible chromophores are phenacyl esters, *o*-nitrobenzyl, coumarin-4-ylmethyl, and its derivatives, pyrenylmethyl and 2-naphthoquinone-3-methide (Figure 1). A reaction initiated by light irradiation depends on the chromophore type and its position in the polymer chain and includes cleavage of photolabile groups from the polymeric chain and consequent depolymerization and chain shortening (if chromophores are introduced into the main chain) or charge and active radical generation or catalyst activation (mainly if inserted into side chains).[1] Irreversible chromophores are advantageous in terms of photoconversion ratio that theoretically may reach 100% as there is no equilibrium between two states (two isomorphs) to establish.[9] Irreversible photochromism is very useful in biomedicine or photolithography, whereas reversible transformations are usually applied in separation applications.

If the changes in a chromophore molecule can be reversed by exposure to a particular light wavelength and sometimes heat, such a compound falls into the category of reversible chromophores (also called photoswitchable compounds or molecular photoswitches). Azobenzene, spiropyran and spirooxazine, diarylethene, triphenylmethane, fulgide and thiophenylfulgide, overcrowded alkene, viologen, stilbene (Figure 1), and coumarin are known as molecular switches.[1,10] The intrinsic ability of the molecule to switch between its isomerization forms back and forth many times, with the number of cycles depending on a photofatigue resistance of the molecule, represents the main advantage of photoswitches as they can be employed in the fields of electro- and optical materials, as sensing devices, in separation processes including gas separation and storage applications.

Isomeric forms of the above-mentioned compounds are shown in Figure 1. Among them, azobenzene and spiropyran were probably studied the most followed by diarylethene, stilbene, and viologen, thus, the description of those compounds' properties can be found elsewhere.[10−15] In this section, we briefly discuss the photoisomerization conditions and differences of isomeric forms of the most widely used compounds, including azobenzene (AZB), spiropyran (SP), and diarylethene (DAE), to illustrate the principles of membrane photoresponsivity.

2.1. Azo Compounds. Azo group compounds ("diazene" in the nomenclature) are characterized by a −N═N− linkage that bridges two or more moieties. Being aromatic compounds, azo compounds have the moieties presented by aromatic rings such as benzene, naphthalene, heterocycles, and others. Bridged by the above-mentioned linkage, the two aromatic rings form a core azo functional structure. Azo compounds typically possess bright colors that are attributed to the strong light adsorption in the visible (vis) region of the spectra (300−700 nm). It is possible to cover the full spectrum of colors by changing the azo molecular design, which determined a special interest in azo compounds by dye industry.[16]

In terms of phototriggered isomerization, three azo compound types are distinguished: (1) azobenzene, (2) aminoazobenzene, and (3) pseudostilbene that appear with yellow, orange, and red colors, respectively, due to the strong light absorption in the corresponding ranges of the spectrum. All of them are subjected to changes in stereochemical conformations of the molecule between *trans*- and *cis*-states but differ in transition band types. For azobenzene and aminoazobenzene compounds, these specific transitions take place either in UV or in vis regions, and absorption spectra of the two isomers do not overlap, which practically means that different wavelengths are required to initiate a transition between isomers, whereas a single wavelength can be used to switch between pseudostilbene isomers.[17,18] However, for all of them, the photoisomerization does not lead to a distinct color change of a material, unlike for other photoresponsive compounds, which is due to the above-mentioned closeness of absorption regions.[19]

Azobenzene (AZB) is the simplest aromatic azo compound, and it was the first one with observed *trans*−*cis* isomerization. The *trans* ("*E*", planar) isomer represents a more stable form as it corresponds to the energy minimum of the ground state,

https://doi.org/10.1021/acsapm.2c00090
ACS Appl. Polym. Mater. 2023, 5, 1−30

Table 1. Properties of the Most Studied Photoresponsive Isomers and Resulting Changes in Gas Separation Membrane Characteristics

compound	more thermodynamically stable form	transition	less stable isomer
	trans ("*E*")		*cis* ("*Z*")
azobenzene (AZB)	properties of the isomer:[33]	UV [300−400 nm][4] ⇆ vis [>400 nm] or heat	properties of the isomer:[33]
	intense $\pi-\pi^*$ band in the UV region		weak n−π^* band in the vis region
	planar geometry		nonplanar geometry
	rod-shaped (distance between *para* carbon atoms is 9.0 Å)		bent-shaped (distance between *para* carbon atoms is 5.5 Å)
	dipole moment 0.5 D		dipole moment 3.1 D
	more hydrophilic		more hydrophobic
	spiropyran ("SP")		merocyanine ("MC")
spiropyran	properties of the isomer:	UV [200−400 nm][38] ⇆ vis [500−600 nm] or heat[40]	properties of the isomer:
	closed-ring form		opened-ring form
	nonplanar (orthogonal) geometry[33]		planar geometry[33]
	π-electrons between two heterocyclic moieties in the SP cannot move[25]		π-electrons between two heterocyclic moieties in the SP are conjugated[25,41]
	not electrically conductive[38]		zwitterionic: phenolate anion and indolium cation[22]
	neutral[23]		Polar
	nonpolar[23]		dipole moment 17.7 (14−18) D[22,33]
	dipole moment 4.3 (4−6) D[22,33]		intensively colored
	colorless[23]		hydrophobic
	hydrophilic[39]		

whereas the *cis* ("*Z*", nonplanar) isomer is attributed to a higher energy level, and that is why, in solutions, the *cis*-form tends to convert back to the *trans*-form.[20] "Destabilization" of the energetically favored state requires higher energy input, which explains why *trans*−*cis* transition happens under exposure to UV light, whereas for the backward trans-formation, visible light or transferred heat energy is enough. Once irradiated by UV light, the *trans*-molecule absorbs the energy, which causes excitation and transition of electrons from a low-energy orbital to an unoccupied high-energy orbital in the aromatic azo core structure. This results in the structural changes in the molecule that switches to its *cis*-state.[16] More details on the structural features of isomers of azobenzene and further described spiropyran along with conditions needed for the transition to occur are presented in Table 1.

2.2. Spiropyran. Spiropyran compounds are characterized by the presence of a benzopyran moiety which linked to a heterocyclic moiety (typically an indoline), via a spiro-carbon atom ("spiro" comes from sp^3 hybridization).[21] Upon exposure to UV light, the excited spiropyran ("SP") undergoes a heterocyclic ring cleavage, which opens the ring and leads to *cis*−*trans* isomerization of the benzopyran double bond, resulting in the formation of a zwitterionic merocyanine ("MC") form containing a phenolate anion and a positively charged indolium.[22] Meanwhile, MC can be transformed back to SP with vis light irradiation or heat.[23] The SP isomer is colorless, which is due to the absorption occurring in the UV region between 200 and 400 nm,[24] whereas the MC absorption spectrum experiences a significant red shift, making MC absorb in the vis region with absorption maxima at 550−600 nm, and hence, it is intensively colored.[25]

Along with photochromism, spiropyran exhibits sensitivity and the ability to respond to other stimuli among which are temperature (thermochromism), pH (acidochromism), solvent nature (solvatochromism), presence and binding of metal ions, redox potential, and mechanical stimulation. The instability of the MC isomer in aqueous solutions is a well-known issue,[26] where MC undergoes hydrolytic decomposition due to a possible nucleophilic water attack. Therefore, it was proposed to reduce the vulnerability of the carbon−carbon double bond by increasing the surrounding electron density.[27] Another concern is a limited reversibility of SP-based molecular switches due to a lower photofatigue resistance of the SP compounds. There are several routes to enhance the fatigue resistance that will be proposed in a following section. One of the options for spiropyrans involves binding of the nitrogen in the indoline moiety by its covalent attachment with a polymeric support material.[28]

2.3. Diarylethene. The diarylethene (DAE) family of compounds represents derivatives of stilbene obtained by replacing stilbene phenyl rings with five-membered heterocyclic rings of lower energy. That contributes to enhancement of thermal stability of both DAE isomers (isomer's half-life time exceeds 400,000 years at room temperature)[12] and greatly increases photofatigue resistance and overall number of photoisomerization cycles (more than 10,000 times).[29] In addition, DAE possesses a high level photoconversion yield that typically exceeds 90%.[12,30]

Diarylethene has an opened-ring colorless form and a closed-ring colored isomer. Irradiation of the open-ring form with UV light causes the ring to close by forming a bond between the two heterocyclic thiophenes. As the absorption spectra shift to a longer wavelength, the closed-ring isomer gains color. Apart from the color change, the geometry of a molecule undergoes a change in height (increases from 0.49 to 0.56 nm) and width (decreases from 1.01 to 0.90 nm), which overall results in a thinner molecule. The back transformation requires visible light. Similar to AZB, it is possible to functionalize DAE in a way that allows these derivatives in dissolved or in crystalline form to obtain colors covering the full color spectra once irradiated with UV light.[12]

2.4. Other Compounds. The irradiation of spirooxazine by UV light initiates similar reactions as described for spiropyrans: the closed-ring spiro-isomer undergoes electrolytic ring opening followed by a molecular rotation,[31] which results in considerable mechanical movement that causes changes in molecular geometry and formation of the highly conjugated mero-form.[32] Exposure of transparent triphenyl-

https://doi.org/10.1021/acsapm.2c00090
ACS Appl. Polym. Mater. 2023, 5, 1−30

methane isomers to UV spectra induces dissociation of triphenylmethane groups into an ion pair, which ends up in the formation of intensively colored cationic forms.[33] UV excitation of fulgides causes closing of the six-membered ring in the fulgide structure within its core and results in the colored isomer formation.[13] Photochromism of naphthalenediimides (NDI) is associated with the appearance of new absorption bands and, hence, a significant color change that occurs through photoinduced electron transfer that converts NDI into NDI radicals.[34] For viologens, once exposed to light, they are subjected to photoinduced electron transfer to a dication form to a counteranion.[35]

There are several photoswitchable compounds among those mentioned above that are being ascribed to a separate group of cycloaddition polymers according to the chosen synthetic route. These compounds are coumarin, stilbene, cinnamic acid, thymine, and anthracene.[10] For example, upon exposure to UV wavelength longer than 350 nm (versus shorter than 260 nm required for reverse transformation), coumarin, which also responds to changes in temperature, undergoes photodimerization reactions in which cyclobutane rings are produced, and a colorless isomer transforms into a colored one.[36] Anthracenes, upon UV light irradiation, undergo [4 + 4] photocycloaddition dimerization,[37] while the same conditions lead to [2 + 2] cycloaddition in stilbenes, resulting in a mixture of stereoisomers of substituted cyclobutane. Another possible photoinduced reaction in stilbenes, even though less favorable, is $E \rightarrow Z$ isomerization.[11]

2.5. Photofatigue-Resistant Chromophores. Photofatigue resistance represents the ability to enter a photoirreversible state, in other words, to maintain the set isomerization state without reverse relaxation and without being subjected by light of a proper wavelength or heat within a specific time, which has a positive effect on material lifetime. Only few photochromes are naturally capable to repeat photoinduced isomerization back and forth more than 1000 times.[12] To increase fatigue resistance of a membrane, the following approaches may be applied: to choose a chromophore with intrinsically higher fatigue resistance properties, to interlink a photoswitch with another moiety that assures enhancement of the property, or to invent unusual molecular design strategies.

Among the available photoswitches, diarylethene (DAE),[12,42] azobenzene (AZB) derivatives,[43] spirooxazine,[31] and naphthopyrans[44] are known for greater fatigue resistance, and thus they were introduced into the materials to enhance the resistance of the membranes. Diarylethenes are ones of the most photofatigue-resistant compounds due to their ability to repeat isomerization cycles more than 14,000 times.[12,29] This number can be further increased by implementing one of the aforementioned strategies, e.g., via introducing acetyl groups into the molecular structure,[45,46] which are proposed to suppress the photochemical C−S bond cleavage. Spiropyrans,[28] Diels−Alder-type cycloaddition polymers,[47] fulgides,[48] and stilbenes,[49] on the contrary, possess much lower resistance. In such cases, more resistant units, in particular, ferrocene moieties, can be covalently linked to chromophores to improve fatigue resistance and other photomodulated properties including photobleaching, irreversibility of photoswitch reactions, and photooxidation, by means of intramolecular interactions.[50] Alternatively, changes in molecular design may also be applied to strengthen material fatigue resistance. As an example, introducing multiple groups of the same chromophore into a polymer repeat unit instead of a single one[51] or interposing a sensitizer building block with a narrow singlet−triplet energy gap to a photochrome building block of, e.g., diarylethene[52] are among the verified approaches.

3. PHOTORESPONSIE MEMBRANE SYNTHESIS AND GAS SEPARATION PERFORMANCE

3.1. Characteristics Desired for Photoresponsive Gas Separation Membranes. An "ideal" photoresponsive gas separation (GS) membrane represents a material with improved desired properties and eliminated defects. Regarding membrane performance, improved permselectivity, i.e., higher selectivity accompanied by higher permeability, is the most treasured achievement. GS membrane materials need to possess good mechanical (including absence of brittleness), chemical, and thermal stability, high resistance toward a humid atmosphere or vapor, and eliminated aging, plasticization, and swelling effects. In the case of inorganic−organic composite membranes, the additional requirements concerning the inorganic−organic material interphase appear. Namely, good compatibility between inorganic filler and organic polymer is desired to ensure uniform dispersion of the filler within the doped polymer and stronger interaction between the phases that minimizes interface voids around the inorganic filler or, on the contrary, polymer penetration into the filler's porous space as well as particles' agglomeration/sedimentation. These requirements are not specific for photoresponsive but are rather common for all GS membranes, and variety of approaches to face the listed issues were summarized in the following review papers.[53−56]

Along with the above-mentioned membrane characteristics, photoresponsive membranes are required to demonstrate good, fast, and complete response once exposed to light irradiation. To obtain that, location and the amount of introduced chromophore units need to be controlled. Since one-direction isomerization is often triggered by exposure to the UV spectra, with a shorter wavelength reducing penetration depth,[57,58] the reasonable strategy is to aim at introducing photoresponsive moieties onto the membrane surface. Chromophores are expected to be uniformly distributed in the membrane separation layer in sufficient amount that is neither too low (leads to a weak response) nor too high (results in chromophore chains overlapping/entanglement decreasing their mobility). The resulting uniformed response of higher amplitude contributes to a higher degree of conversion of light energy to photoinduced changes in the membrane. Elimination of the photofatigue effect allows chromophores to maintain a sufficient response for a higher number of photoisomerization cycles, which increases the overall membrane uptime. Furthermore, good thermal stability is required in cases when the back-isomerization is stimulated by heat.[59]

3.2. Preparation of Gas Separation Membranes. The ultimate membrane separation performance is determined by physical−chemical properties of a membrane material and membrane structure. The latter is predetermined by the properties of pristine membrane materials, solvents, and other chemicals involved in the synthesis, the chosen synthetic techniques, and synthetic conditions. The structure of photoresponsive membranes strongly depends on the architecture of the building unit carrying the photoresponsive moiety, which determines successful photoinduced material response and ultimate separation performance.

https://doi.org/10.1021/acsapm.2c00090
ACS Appl. Polym. Mater. 2023, 5, 1−30

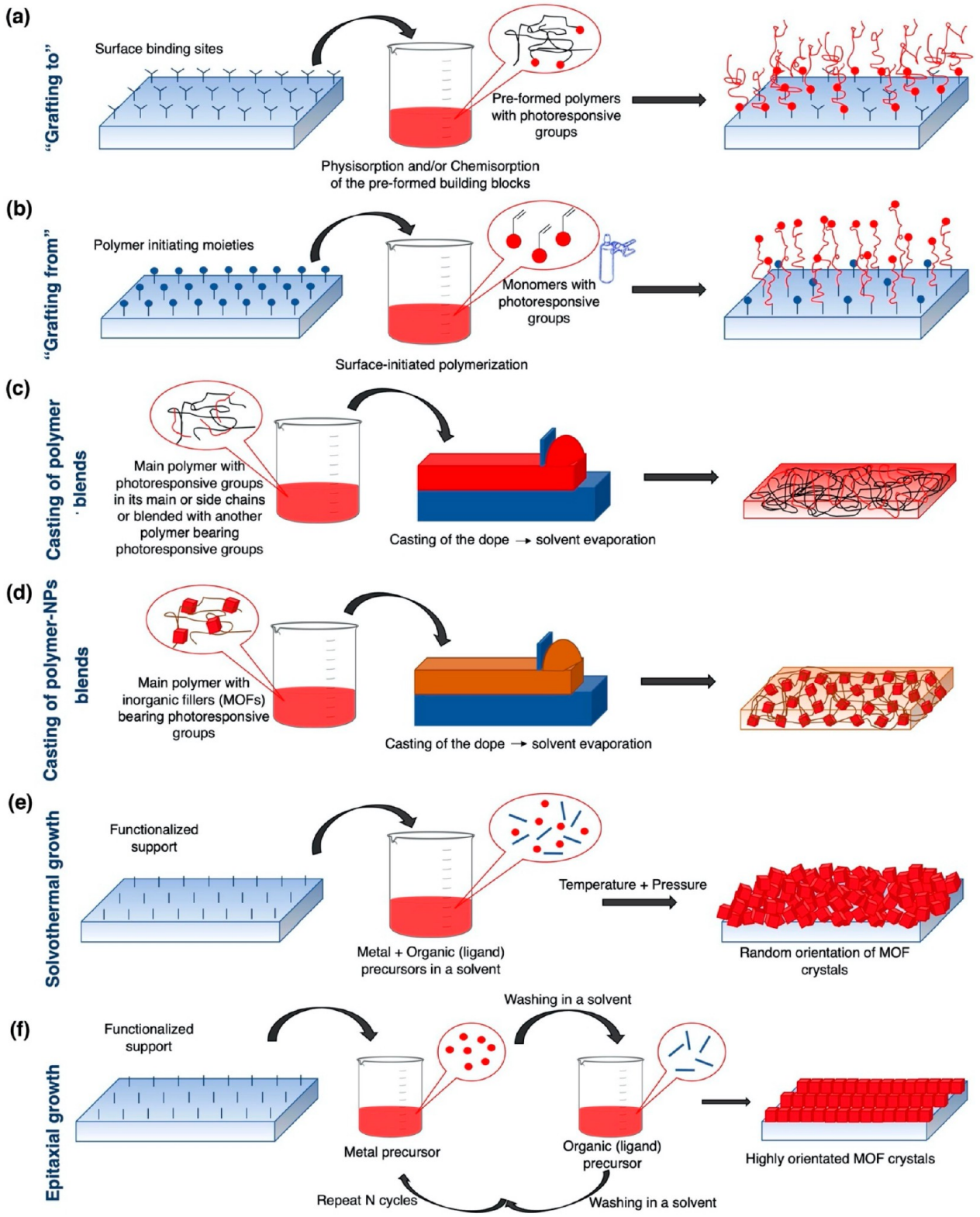

Figure 2. Schematic illustration of the techniques applied in synthesis of photoresponsive gas separation membranes. Polymeric membranes: grafting to (a); grafting from (b); and blending−casting−solvent evaporation (c). MMMs: blending−casting−solvent evaporation (d). MOF thin films: solvothermal deposition (e) and liquid-phase epitaxial growth (f).

Photoresponsive GS membrane fabrication represents a novel research direction, which explains the relatively low number of publications on the topic. The synthesis approaches mostly rely on casting of a polymeric film subjected to solvent evaporation (polymeric or mixed-metal membranes (MMMs)), modification of the separation layer of a precasted membrane via grafting procedure, or growing of a MOF thin film onto a pretreated support material. Schematic illustrations of synthetic techniques applied in the preparation of photoresponsive GS membranes are given in Figure 2. Slow

https://doi.org/10.1021/acsapm.2c00090
ACS Appl. Polym. Mater. 2023, 5, 1−30

Table 2. Gas Separation Performance of the Reviewed Photoresponsive MOF-MMMs, MOF Thin Films, and Polymeric Membranes

MOF	BET SA (m^2/g)	pore volume (cm^3/g)	gas uptake at (1 bar)	CO_2/N_2 selectivity at 1 bar	MMM	CO_2 permeability[a] (Barrer at 1 bar)	CO_2/N_2 ideal selectivity[a]	ref
Gen-2 MOFs					**Gen-2 MOF-MMMs**			
DMOF-1	1500	0.79	$CO_2[cm^3/g]$	na	neat PIM-1	4000/3200[b]	15/10[b]	88
			273 K: 90.0		PIM-azo-DMOF (5 wt %)	6700	20	
			298 K: 43.0		PIM-azo-DMOF (10 wt %)	7500	19	
					PIM-azo-DMOF (20 wt %)	10000/7600[b]	17/14[b]	
azo-DMOF-1	581	0.3	$CO_2[cm^3/g]$	na	neat Matrimid	6.7	29	
			273 K: 73.0					
			298 K: 41.0					
			CO_2 under UV					
			273 K: 36.0		Matrimid-azo-DMOF (5 wt %)	9.6	36	
			298 K: 29.0		Matrimid-azo-DMOF (10 wt %)	13	50	
UiO-66	983	0.64	CO_2[mmol/g]	273 K: 25	neat Matrimid	6.0	31	89
			273 K: 2.77	298 K: 25		UV: 5.9		
			298 K: 2.17					
			N_2		Matrimid-UiO-66 (10 wt %)	11.1	29	
			273 K: 0.31			UV: 11.0		
			298 K: 0.15					
azo-UiO-66	394	0.35	CO_2[mmol/g]	273 K: 37	Matrimid-azo-UiO-66 (5 wt %)	7.1	35	
			273 K: 1.38	298 K: 100		UV: 6.6		
			298 K: 0.76		Matrimid-azo-UiO-66 (10 wt %)	10	37	
			N_2			UV: 9.4		
			273 K: 0.13		Matrimid-azo-UiO-66 (20 wt %)	12.8	40	
			298 K: 0.03			UV: 11.8		
UiO-66	1005	0.51	CO_2[mmol/g]	298 K: 97	neat PIM-1	7500/6600[c]	13.5/11.4[c]	90
			298 K: 2.16					
			N_2		PIM-azo-UiO-66(10 wt %)	13000/10000[c]	13.5/11.5[c]	
			298 K: 0.14					
azo(16.7)-UiO-66[d]	821	0.41	CO_2[mmol/g]	298 K: 119	PIM-azo (16.7)-UiO-66(10 wt %)	13000/9000[c]	15.5/12.8[c]	
			298 K: 2.24/2.10					
			N_2					
			298 K: 0.182					
			CO_2 under UV					
			298 K: 1.75					
azo(33.3)-UiO-66[d]	684	0.35	CO_2[mmol/g]	298 K: 117	PIM-azo (33.3)-UiO-66(10 wt %)	13000/8500[c]	15.0/13.4[c]	
			298 K: 2.14/1.80					
			N_2					
			298 K: 0.138					
			CO_2 under UV					
			298 K: 1.41					
azo(66.7)-UiO-66[d]	586	0.29	CO_2[mmol/g]	298 K: 49	PIM-azo (66.7)-UiO-66(10 wt %)	11000/9000[c]	16.5/13.0[c]	
			298 K: 1.07/0.85					
			N_2					

https://doi.org/10.1021/acsapm.2c00090
ACS Appl. Polym. Mater. 2023, 5, 1−30

Table 2. continued

MOF	BET SA (m^2/g)	pore volume (cm^3/g)	gas uptake at (1 bar)	CO_2/N_2 selectivity at 1 bar	MMM	CO_2 permeability[a] (Barrer at 1 bar)	CO_2/N_2 ideal selectivity[a]	ref
			298 K: 0.094 CO_2 under UV 298 K: 0.58					
azo(100)-UiO-66[d]	382	0.18	CO_2[mmol/g] 298 K: 0.63/0.76 N_2 298 K: 0.045 CO_2 under UV 298 K: 0.57	298 K: 30	PIM-azo (100)-UiO-66(10 wt %)	11000/9300[c]	19.5/18.2[c]	
	G-3 MOFs					**G-3 MOF-MMMs**		
JUC-62	1020	na	CO_2[cm^3/g] 273 K: 146	na	neat Matrimid	9.5 UV: 9.4	32.7	91
					Matrimid-JUC-62(5 wt %)	11.0 UV: 10.3	37.9	
					Matrimid-JUC-62(10 wt %)	26.3 UV: 25.0	40.5	
					Matrimid-JUC-62(15 wt %)	30.5 UV: 27.9	56.5	
PCN-250	1376	na	CO_2[cm^3/g] 273 K: 107	na	Matrimid-PCN-250(5 wt %)	18.5 UV: 17.4	37.0	
					Matrimid-PCN-250(10 wt %)	29.8 UV: 28.5	64.1	
Co(AzDC) [MW]	874	0.35	SO_2[cm^3/g]2 h 273 K: 230 295 K: 165 SO_2 under UV 273 K: 220 295 K: 140 SO_2[cm^3/g]10 h 273 K: 370 295 K: 290 SO_2 under UV 273 K: 300 295 K: 200		neat PI (Matrimid)	CO_2 dry: 6.5 wet: 60 SO_2: 26 SO_2 UV: 26	CO_2/N_2 dry: 32 wet: 32 SO_2/N_2: 130 SO_2/N_2 UV: 130	92
					PI-Co(AzDC)(5 wt %)	CO_2 dry: 8.4 wet: 80	CO_2/N_2 dry: 35 wet: 40	
					PI-Co(AzDC)(10 wt %)	CO_2 dry: 11.7 wet: 155 SO_2: 44 SO_2 UV: 28	CO_2/N_2 dry: 70 wet: 77 SO_2/N_2: 440 SO_2/N_2 UV: 280	
					PI-Co(AzDC)(20 wt %)	CO_2 dry: 5.6 wet: 175	CO_2/N_2 dry: 49 wet: 55	
					PI-Co(AzDC)(30 wt %)	CO_2	CO_2/N_2	

https://doi.org/10.1021/acsapm.2c00090
ACS Appl. Polym. Mater. 2023, 5, 1−30

Table 2. continued

MOF	BET SA (m^2/g)	pore volume (cm^3/g)	gas uptake at (1 bar)	CO_2/N_2 selectivity at 1 bar	MMM	CO_2 permeability[a] (Barrer at 1 bar)	CO_2/N_2 ideal selectivity[a]	ref
						dry: 9.7	dry: 38	
						wet: 225	wet: 46	
		COPs				**COP-MMMs**		
azo-COP-2	554	0.175	CO_2[mmol/g]	na	neat Matrimid	10.0	23.0	99
			273 K: 2.12		Matrimid-azo-COP-2(5 wt %)	14.9	24.6	
			298 K: 1.28		Matrimid-azo-COP-2(10 wt %)	17.1	26.3	
			SO_2[mmol/g]		Matrimid-azo-COP-2(15 wt %)	27.1	22.2	
			273 K: 1.66					
			298 K: 1.05		neat PS	5.7	13.7	
					PS-azo-COP-2(5 wt %)	6.3	15.7	
					PS-azo-COP-2(10 wt %)	10.4	22.1	
					PS-azo-COP-2(15 wt %)	14.8	22.8	
					neat PIM	4500	14.0	
					PIM-azo-COP-2(5 wt %)	5500	16.0	
					PIM-azo-COP-2(10 wt %)	7000	14.3	
					PIM-azo-COP-2(15 wt %)	10500	12.0	
	MOF thin films				**polymeric membranes**			
neat UiO-67 onto α-Al_2O_3 support	permeance, 10^{-7} mol·s^{-1}·$(m^2)^{-1}$·Pa^{-1}:		selectivity:	104	neat PMMA	*trans/cis* permselectivity at 298:		2
	H_2: 10.20		H_2/CO_2: 8.7			H_2: 1.025		
	CO_2: 1.17					n-C_4H_{10}: 1.05		
						CH_4: 1.0		
						SF_6: 1.025		
						CH_3OH: 1.0		
azo (19 wt %)-UiO-67 onto α-Al_2O_3 support (Gen-1 MOFs)	[*trans*]:		[*trans*]:		PMMA/AZB/blended	*trans/cis* permselectivity at 298:		
	H_2: 4.41		H_2/CO_2: 14.7			H_2: 1.0		
	CO_2: 0.30		[*cis*]:			n-C_4H_{10}: 1.0		
	[*cis*]:		H_2/CO_2: 10.1			CH_4: 1.0		
	H_2: 5.10					SF_6: 1.0		
	CO_2: 0.51					CH_3OH: 0.8		
					PMMAZB/side chain	*trans/cis* permselectivity at 298:		
						H_2: 1.15		
						n-C_4H_{10}: 1.3		
						CH_4: 1.7		
						SF_6: 4.0		
						CH_3OH: 0.7		
					PMD77/side chain	dark/blue light flow rate, mL/min:		62
					azoPMD-1(2.5 wt %)	0.57/0.62		
					azoPMD-2(1.0 wt %)	0.40/0.44		
Cu_2(azoBPDC)$_2$(azoBiPyB) (Gen-2 MOFs)	permeance, 10^{-7} mol·s^{-1}·$(m^2)^{-1}$·Pa^{-1}:		selectivity:	85	PI/coPI	N_2: 0.089/0.290	O_2/N_2: 6.9/6.3	64
	H_2: 1.3		[*trans*]:			O_2: 0.617/1.820	He/N_2: 160/94	
	CO_2: 1/0.3[*trans/cis*]		H_2/CO_2: 3.0			He: 14.2/27.2	CO_2/N_2: 30.3/27.2	

https://doi.org/10.1021/acsapm.2c00090
ACS Appl. Polym. Mater. 2023, 5, 1−30

Table 2. continued

MOF	BET SA (m^2/g)	pore volume (cm^3/g)	gas uptake at (1 bar)	CO_2/N_2 selectivity at 1 bar	MMM	CO_2 permeability[a] (Barrer at 1 bar)	CO_2/N_2 ideal selectivity[a]	ref
	N_2: 9.1		N_2/CO_2: 5.4			CO_2: 2.70/7.89		
	CO_2: 1.2/1[*trans/cis*]		[*cis*]:					
			H_2/CO_2: 8.0		azo-PI/azo-coPI/blended	N_2: 0.012/0.086	O_2/N_2: 10.0/6.9	
			N_2/CO_2: 8.3			O_2: 0.120/0.596	He/N_2: 388/160	
						He: 4.7/13.8	CO_2/N_2:	
						CO_2: 0.45/2.30	37.1/26.7	
						UV:	UV:	
						N_2: 0.011/0.085	O_2/N_2: 8.6/6.3	
						O_2: 0.094/0.532	He/N_2: 399/155	
						He: 4.4/13.2	CO_2/N_2: 29.0/21.9	
						CO_2: 0.32/1.86		
					azo-PI/azo-coPI/side chain	N_2: 0.058/0.171	O_2/N_2: 9.3/5.7	
						O_2: 0.540/0.966	He/N_2: 174/76	
						He: 10.1/13.0	CO_2/N_2:	
						CO_2: 2.28/4.20	39.3/24.6	
						UV:	UV:	
						N_2: 0.051/0.167	O_2/N_2: 8.6/5.3	
						O_2: 0.437/0.879	He/N_2: 200/76	
						He: 10.2/12.7	CO_2/N_2: 33.3/22.2	
						CO_2: 1.70/3.70		
$Cu_2(F_2azoBDC)_2(dabco)$ (Gen-2)	permeance, 10^{-7}·mol·s^{-1}·$(m^2)^{-1}$·Pa^{-1}:		selectivity:	107	neat PI	N_2: 0.048	O_2/N_2: 7.12	63
			[*trans*]:			O_2: 0.342	CO_2/N_2: 29.23	
	H_2: 7.5		H_2/C_2H_4: 6.6		azo-PI/backbone	He: 5.84		
	C_2H_4: 0.75/1[*trans/cis*]		H_2/C_3H_6: 8.2			CO_2: 1.40		
			[*cis*]:			[*trans*]:	[*trans*]:	
	H_2: 4.5		H_2/C_2H_4: 8.8			N_2: 0.077	O_2/N_2: 6.94	
	C_3H_6: 0.4/0.6[*trans/cis*]		H_2/C_3H_6: 12.6			O_2: 0.534	CO_2/N_2:29.61	
						He: 7.91		
						CO_2: 2.28		
						UV [*cis*]:	UV [*cis*]:	
						N_2: 0.072	O_2/N_2: 7.25	
						O_2: 0.522	CO_2/N_2: 29.17	
						He: 7.78		
						CO_2: 2.10		

[a]The values correspond to the single-gas permeation measurements of others not indicated. [b]For the equimolar CO_2/N_2 gas mixture scenarios. [c]For the gas mixture scenarios of 15/85 CO_2/N_2. [d]In azo(X)-UiO-66, X stands for the percentage of the azo-modified linker (2-phenyldiazenyl terephthalic acid).

https://doi.org/10.1021/acsapm.2c00090
ACS Appl. Polym. Mater. 2023, 5, 1−30

solvent evaporation results in dense symmetric membranes with more rigid structure if photoresponsive groups are a part of the main polymer chain or, on the contrary, denser matrix if photoswitches are side-chained or blended with the main polymer (Figure 2c). Grafting of the chromophores onto the membrane surface does not affect the film density but enhances the mobility of photoresponsive units (Figure 2a,b). The structure of MMMs obtained via solvent evaporation is much more porous than that of polymeric membranes due to the inorganic fillers dispersed in the matrix (Figure 2d). Here, the architecture of the photoresponsive MOF filler differs depending on the chromophores either being positioned inside the pore of the filler or being a part of its structure (main skeleton or side chain). The same MOF architectures remain in the synthesis of MOF thin films by solvothermal seeding or liquid phase epitaxy. The main structural difference between the two approaches is in the orientation of the MOF crystals being randomly deposited in solvothermal synthesis (Figure 2e) and highly oriented in the epitaxial growth (Figure 2f).

3.3. Synthesis and Performance of Photoresponsive Polymeric Membranes. Preparation of polymeric membranes with a photoresponsive behavior are made via either processing of a polymer synthesized in a way to carry the chosen photoresponsive moieties or postsynthetically modifying the membrane surface by a grafting technique. In the former method, photoresponsive monomers that are converted into polymers, copolymers, or their blends are used as a main component of the doped solution or as an additive to it. A photoresponsive moiety can be introduced as a part of the main polymer chain or as a side chain or to be blended with the main component. In this approach, materials are synthesized to carry photoresponsive units before being processed into membranes, which is different in the case of postsynthetic modification (PSM) of the membrane surface. In PSM, two approaches—"grafting to" and "grafting from"—are distinguished, with the former one introducing preformed responsive molecules onto the membranes' surface and the latter one representing surface-initiated polymerization, during which grafted chains are formed in situ by addition of monomers from the solution.[60]

3.3.1. Membrane Preparation by Blending. In blending, photoresponsive moieties can be linked to a monomer or presented in the backbone, side chains, or as terminal groups of the polymer(s)/copolymers. In addition, membrane fabrication from materials already loaded with photoresponsive units have the advantages of ease of polymer processability. However, hindrance of photochromes' mobility because of their binding with the surrounding polymer matrix or their complete burial into the polymer depth under the skin layer remains an issue. Another challenge is assurance of uniform distribution of the photochrome units within the polymer matrix, which is governed by their uniform distribution in the doped solution. Some intrinsic properties of chromophores may lead to aggregation in solutions (e.g., dipolar nature of AZB compounds). Aggregation might be controlled to some extent by choosing a solvent that is highly compatible with the main polymer and photochrome units and sufficient mixing of the doped solution either by magnetic stirring or by ultrasonication.[61]

A casted polymer blend can be processed into a photoresponsive membrane by radiation curing, (wet) phase inversion, or solvent evaporation techniques. For GS application, only solvent evaporation was reported. A solvent evaporation method (Figure 2a), or solvent casting, includes dissolving a mixture of photoresponsive polymers or copolymers in a proper volatile solvent or a less volatile nonsolvent (typically water or alcohols). The doped solution is then casted onto a glass substrate followed by solvent evaporation and polymer-rich phase enrichment with a nonsolvent that causes polymer film precipitation.[61]

In one of the first studies on photoresponsive gas separation polymeric membranes, reported by Weh et al.,[2] polymethacrylate membranes carrying azobenzene units either in the polymer side chain (PMAZB) or physically blended (PMMA/AZB, AZB = 30 wt %) with the main polymer were fabricated. The doped solution was spin-coated onto an asymmetric UF ceramic membrane (acting as a carrier for the deposited membrane thin film), and the membrane was formed in a slow solvent evaporation process. For the PMAZB membrane, with gas permeability measured at 298 K, ambient conditions (no light irradiation applied) increased in the order of SF_6 < CH_4 < n-C_4H_{10} < H_2 < CH_3OH (the numerical values are presented in Table 2). The light-modulated PMAZB behavior was illustrated by the change in absolute permeability values, which decreased upon exposure of the membrane to UV light. The only exception was methanol, for which permeability increased upon UV irradiation. Switching from *trans*- to *cis*-azobenzene reduces the mean free volume of the polymer matrix as *cis*-isomers represents a more effective obstacle for transport of gas molecules due to their "curled" geometry compared to that of the elongated *trans*-isomers, which explains lower gas permeabilities observed with PMAZB in the *cis*-state.

Gas permeabilities through the PMMA/AZB membrane increased in the order of SF_6 < n-C_4H_{10} < CH_4 < H_2 < CH_3OH (Table 2) and were much lower than those through the PMAZB due to the occupation of the membrane free volume by blended AZB molecules, which reduced gas transport capacity of the polymeric film. In addition to this, the PMMA/AZB membrane did not show photoresponsive behavior as gas permeabilities measured in either the *trans*- or the *cis*-state were the same. Here again, methanol was an exception demonstrating higher flux through the *cis*-state membrane. When introduced by blending, a significant part of chromophores may be "buried" into membrane depth and hence become unavailable to UV light exposure. This may cause an absence of the effect of UV irradiation and thus the hindrance of photoisomerization. However, changes in the reverse pattern for methanol permeability confirmed that at least partial photoswitching took place. Methanol permeability was the highest among all of the tested gases, which is attributed to the higher solubility of polar methanol molecules in the polar PMMA film compared with that in nonpolar gases. Furthermore, the AZB *cis*-isomer possesses a polar nature, which explains the reverse permeability pattern (its increase under UV light) for methanol observed for both PMAZB and PMMA/AZB membranes.

Azobenzene was also introduced into the side chain of PMD77 (a random copolymer of methyl methacrylate and 2-{ethyl-[4-(4-nitrophenylazo)phenyl]amino}ethyl methacrylate) in a previous study.[62] Polymer thin film was spin-coated onto the modified polymeric UF membrane and left for solvent to evaporate forming the dense membrane structure. Concentrations of azopolymer were 2.5, 1.0 and 0.5 wt % in the obtained AzoPMD-1, AzoPMD-2, and AzoPMD-3 membranes, respectively. The highest changes in He

https://doi.org/10.1021/acsapm.2c00090
ACS Appl. Polym. Mater. 2023, 5, 1−30

permeability caused by blue light irradiation were observed in AzoPMD-2, where up to a 10% increase was detected (the measured values are given in Table 2). AzoPMD-1 showed 2-fold lower increase, whereas AzoPMD-3 membrane did not demonstrate light-driven permeability changes. The authors imply the defect-free coverage of azopolymer over the membrane and formation of localized azo particulate domains as necessary for a good photoresponse.

Polymer of intrinsic microporosity (PIM)-based membranes with a diarylethene photoresponsive unit introduced into the polymer backbone were synthesized by coupling of the DAE derivative with spirobifluorene monomers by a Suzuki cross-coupling reaction.[57] The dissolved polymer (DAE in the open form, DAE^{O}-PIM) was drop-casted and subjected to solvent evaporation, forming a thin film. Along with a color change from green-yellow to violet, DAE cyclization triggered by UV light (254 nm) exposure caused a significant decrease in material SA from 395 m^2/g in the initial DAE-open form to 168 m^2/g in the closed form. Cycloreversion reactions initiated by visible light (550 nm), however, made the SA increase to 245 m^2/g, and yet it never reached its initial value. Those corroborated photoresponsive properties of DAE remained once incorporated into PIM and revealed incomplete back-isomerization, which may be due to a partial DAE degradation upon exposure to short and intense 254 nm wavelength (photofatigue resistance). For gas separation experiments, powdered DAE-PIM (5 wt %) was blended with Matrimid to obtain a free-standing film via the casting/solvent evaporation path. Incorporation of DAE-PIM slightly increased CO_2 permeability compared to the pure Matrimid membrane (13 against 10 Barrer), whereas the increase was almost negligible in the case of O_2 (2.9 against 3.1 Barrer). However, after several UV−vis irradiation cycles, the permeability of both CO_2 and O_2 decreased, showing physical aging was taking place. Moreover, since the decrease was getting higher with the number of cycles, it may be also partially attributed to the described DAE degradation, which fixes DAE in the closed form. Lower CO_2 permeability upon exposure to UV light was attributed to a more rigid and planar structure of the closed DAE form, whereas the slightly bent open form creates more free volume between polymer chains composed of a membrane matrix, and thus more pathways are open for gas molecules to be transported.

Azobenzene was introduced into the backbone of polyimide (PI) via two-step polycondensation reactions.[63] A polymer-doped solution was casted onto a Petri dish, and the azo-PI membrane was formed in the solvent evaporation process. Permeability of gases obtained with all membranes—azo-PI in *trans*- and *cis*-forms and pure PI—increased in the order of N_2 < O_2 < CO_2 < He (Table 2 summarizes the obtained numerical data), which corresponds to a decrease of the kinetic diameter of the gas molecules. Further, permeability of all gases increased with azo-PI in the *trans*-form compared to that in the neat PI membrane due to the presence of the rigid −N═N− azo bond (the enhanced rigidity is corroborated by higher T_g values for the azo membranes) with a length of 1.23 Å in its *trans*-configuration in the polymer main structure, which decreases the packing density of polymer chains increasing polymer fractional free volume. When switched to the *cis*-form by illuminating at the wavelength of 405 nm, a slight decrease in permeabilities was observed for all gases; however, the values still enhance those obtained with neat PI. This decrease is attributed to the geometry of *cis*-isomers that provides higher packing density and, thus, less free pathways for gas molecules to travel. A low degree of changes is attributed to insufficient UV irradiation since membrane thickness is much higher than the wavelength penetration depth, as well as a possible partial *cis*-form back-relaxation to a more thermodynamically stable *trans*-isomers.

The work was continued by Nocoń-Szmajda et al.,[64] where azobenzene groups were covalently bonded as polyimide side groups or physically blended with the main polymer. For all of the membranes, permeabilities keep the same order (N_2 < O_2 < CO_2 < He) (Table 2) as found before.[63] However, all azo-bearing membranes showed a permeability lower than that of the neat PI or coPI, which is in direct correlation with polymer T_g values. Particularly, lower T_g indicates that azo functionalization increased polymer chain mobility, and more mobile chains were able to pack in a more space-efficient way, thus reducing free volume and consequently gas permeability. A drop in permeability is even more pronounced for azo-doped (co)PI membranes due to the even higher decrease of polymer free volume via occupation by blended azobenzene. That is opposite to the case when azo moieties were inserted into the polymer main chain, increasing the chain rigidity and polymer free volume and, hence, gas permeability. However, then, azo-doped and azo-functionalized (side-chain) membranes demonstrated a higher degree of photoresponse; i.e., the changes in gas permeability and selectivity under UV irradiation were higher than that for the azo moieties presented into the main chain, most probably, due to the higher mobility of azo groups to undergo geometrical transformations. For all azo-bearing membranes, permeability of the *trans*-form is higher than that for the *cis*-form due to the nonplanar geometry of the *cis*-isomer, which makes it bulkier, and its higher polarity that reveals the possibility of additional dipole−dipole interactions between *cis*-molecules.

3.3.2. Membrane Surface Modification via Grafting. Grafting (Figure 2b) represents a functionalization of membrane surface by photoresponsive moieties, and thus it inherently satisfies the requirement of having photoresponsive groups on the material surface. Among all techniques for polymeric membrane preparation, grafting offers more possibilities to control the moieties' hindrance, as it strongly depends on the parameter of grafting density rather than cross-linking with a polymer matrix. To the best of our knowledge, there are currently no papers covering the preparation of gas separation membranes via surface grafting. However, high versatility of the method generated attention to the grafting in photoresponsive materials for other applications including biomedical and liquid separation,[60] and it might be an interesting direction for the synthesis of GS membranes, as well.

In the "grafting to" approach, preformed molecules/polymer chains with chromophore units introduced as end functionalities were attached to the membrane surface via physical adsorption or chemical grafting. For adsorption to occur, a membrane is soaked into the solution that contains the photoresponsive molecules following the drying procedure and sometimes annealing to strengthen the attachment. In chemical grafting, a reaction between functional groups onto the surface of the membrane and those of photoresponsive polymer chains links them together by forming a chemical bond. In some cases, formation of functional groups onto the membranes' surface may occur along with their bonding with chromophore molecules.[60]

https://doi.org/10.1021/acsapm.2c00090
ACS Appl. Polym. Mater. 2023, 5, 1−30

"Grafting from" allows even better control of chromophore loading ("grafting density") and their more uniform distribution. These groups of methods use monomers embedded with photoresponsive moieties dissolved in a solution as starting materials. There is no preformed polymeric chain; it is going to be grown during the polymerization reaction. Modification starts with immobilization of an initiator onto the membrane surface that is further activated by photo-, γ-, or plasma irradiation or redox reactions. The activation results in the formation of radicals, which initiate and govern the polymerization reaction. Polymerization starts once the membrane is transferred into the monomer solution while irradiation continues. In many cases, an inert atmosphere is a must. Among all of the "grafting from" techniques, the interest is growing toward an atom-transfer radical polymerization (ATRP) approach as it provides the highest control on polymerization reactions, which can be terminated whenever required.[60]

An illustration of the preparation of a photoresponsive membrane via surface grafting is given in the study of Chen et al.,[65] although the synthesized material was applied for oil/water separation. In the study, a commercial polypropylene (PP) membrane underwent plasma purging in an argon atmosphere followed by a polyreaction to introduce poly(acrylic acid) (PAA), leaving a PAA-grafted membrane (PAA-g-PP). PAA was required to further fix ammoniated SiO_2 nanoparticles (NPs) onto the membrane surface to increase its roughness. Then the PP-g-SiO_2 NP membrane was placed in an azo-containing ethanol solution for 3 h followed by washing in either water or ethanol and a drying step. As applicable to liquid separation, a remarkable alteration between superhydrophobicity (maximum CA of 160°) and superhydrophilicity (minimum CA of 5°) was achieved by switching between UV (365 nm) and vis (440 nm) light.

Closer to gas-related applications, Chen et al.[66] reported the preparation of azobenzene-grafted porous stainless steel (SS) membranes (not polymeric). A bare SS membrane was sputter-coated with gold followed by functionalization with carboxyl groups upon soaking in the 11-mercaptoundecanoic acid solution in ethanol and washing steps. Further, the membrane was immersed into the ethanol solution containing *p*-aminoazobenzene, and azobenzene photoswitches were grafted onto the membrane surface via amine bond formation in the presence of a catalyst. The formed membrane was applied as liquid gates (LCGV, light-responsive and corrosion-resistant gas valve) for controllable gas flow (see Figure 3). When no UV light is applied, strong interactions between the *trans*-azobenzene located on the surface of the solid membrane and the nonpolar gating liquid and a small gas pressure difference between both sides of the pore keeps the pore closed, and thus, the gas flow is restricted. However, exposure to UV light causes azobenzene molecules to undergo *trans*-to-*cis* photoisomerization, which significantly increases the polarity of the molecules and consequently weakens their interactions with the nonpolar gating liquid. This decrease of the solid−liquid interaction reduces the critical gas pressure in the system and opens the pore for gas transport. Although the working mechanism relied on the interactions between photoswitches and the liquid phase, the obtained results were beneficial for gas-related applications such as transportation of natural gas, degassing, a variety of gas-involved processes, and gas sensors.

3.4. Synthesis and Performance of Photoresponsive MOF−Polymer MMMs. Mixed-matrix membranes were designed to merge the benefits of polymeric and inorganic membranes into one material along with elimination of the ascribed drawbacks. As such, MMMs inherited improved thermal, chemical, and mechanical properties from the inorganic filler part and diminished swelling and plasticization characteristics of the organic polymer phase. However, the most important advantage is enhanced gas separation performance (above the Robeson's upper bound).[53]

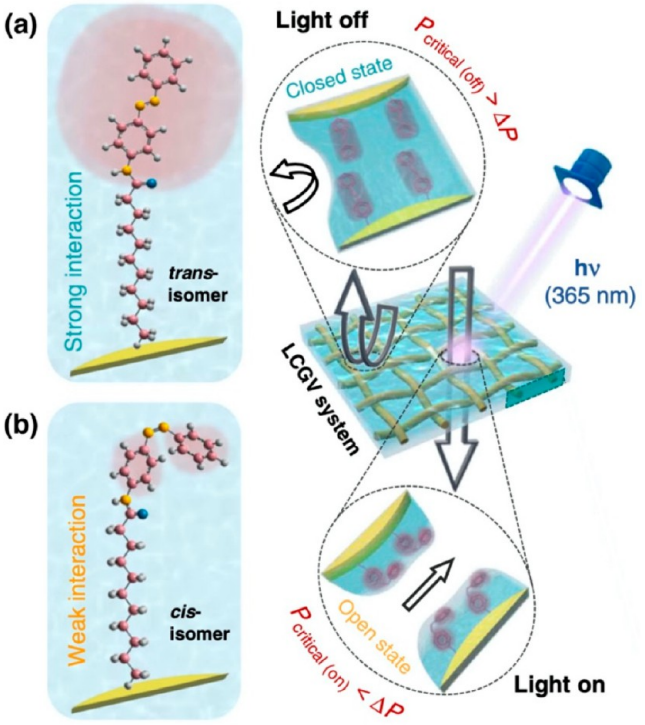

Figure 3. Schematic view of the working principle of the light-responsive corrosion-resistant gas valve LCGV: LCGV in a closed (a) and opened (b) states. Reprinted in part with permission from ref 66. Copyright 2021 Springer Nature.

The most applied method to fabricate MMMs is physical blending and sol−gel approach; however, the latter has not yet been reported for photoresponsive GS membrane synthesis. MMMs' blending represents the same approach as described for polymeric membrane preparation with the only extension of adding presynthesized inorganic nanoparticulate fillers in the blend prior to its casting (Figure 2c).[61] Solvent evaporation might be followed by membrane annealing to strengthen binding between polymeric and inorganic phases. The photoresponsive property of MMMs can originate from a polymer that composes a membrane continuous phase. However, a more reasonable approach would be for fillers to carry photoresponsive moieties. A variety of materials can be applied as fillers in MMMs, of which MOFs are being the most widely studied in terms of carrying photoresponsive compounds.

MOFs belongs to a class of coordination network structures which is, in this case, a subset of coordination polymers. The hierarchy is chaired by coordination compounds. According to the IUPAC definition, coordination compounds are those that contain any coordination entity. The coordination entity consists of an ion or neutral molecule with a central atom (usually represented by a metal) surrounded by an attached array of [groups of] atoms or groups of atoms (ligands).

https://doi.org/10.1021/acsapm.2c00090
ACS Appl. Polym. Mater. 2023, 5, 1−30

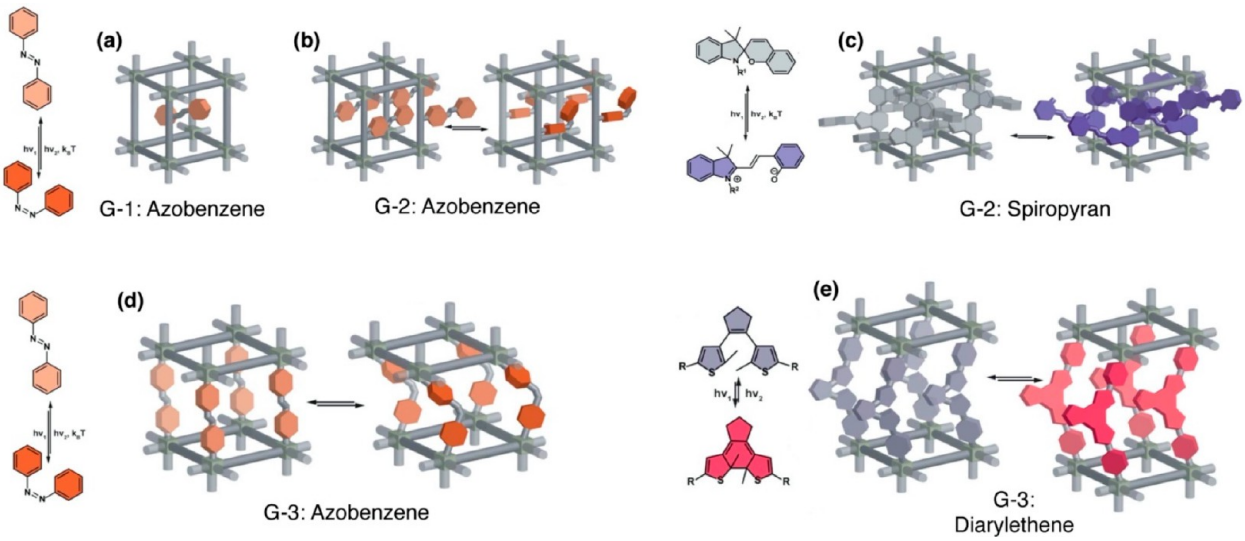

Figure 4. Schematic view of the structures of photoresponsive MOFs: generation 1 (G-1) (a), generation 2 (G-2) (b,c), and generation 3 (G-3) (d,e). Reprinted in part with permission from ref 11. Copyright 2020 The Royal Society of Chemistry.

Coordination compounds can be divided on discrete and polymeric (i.e., consisting of repeating units) compounds. Coordination polymers (CPs) are then distinguished as 1D CPs (linear chain polymers), and 2D/3D CPs are called coordination networks. There is no strict definition for MOFs; however, for the start, the requirement of potential voids should be fulfilled.[67]

MOFs are mostly built from metal cations (usually d- or f-block elements) and organic ligands that bridge metal centers, thus creating inorganic polymeric structures extended in three dimensions. MOFs can be loaded with photochromes as guest molecules at a postsynthetic stage or being synthesized in a way in which the ligand carries the photoresponsive units as a side group or as a part of its backbone. Based on the position of the chromophores in the framework structure, three generations of photoresponsive MOFs are distinguished. They are depicted in Figure 4.

3.4.1. Photoresponsive MOFs: Generation 1. 3.4.1.1. Generation 1 MOFs. Generation 1 (Gen-1) MOFs are described as having photochromic molecules loaded into the cage of presynthesized MOFs (Figure 4a), which results in a distortion of the cage changing its structure upon light irradiation. Presynthesis of MOFs is performed via the same routes as those for non-photoresponsive frameworks: conventional at lower temperatures and solvothermal at elevated temperatures, sono-, electro-, mechanochemical, and microwave-assisted that were discussed elsewhere.[68,69] Embedment of chromophores into the framework's pores is usually done via gas-phase loading. The process is performed for several hours under vacuum/reduced pressure and elevated temperatures.[70,71] Not only "pure" chromophores but also modified ones can be used to tailor the final MOF for a specific application. For example, azobenzene molecules can be fluorinated to separate the absorption bands of *E* and *Z* isomers, which otherwise overlap, causing a prohibition of complete photoswitching between the isomeric form.[72] Azobenzene, diarylethene, spiropyran, viologen, anthracene, and stilbene were investigated as guest molecules in MOFs in a variety of applications.[42] Gen-1 frameworks were tested in a powder form or as thin films (section 3.5) owing to the guest introduction procedure, which is inefficient to perform with a polymeric membrane. Currently, for gas separation, Gen-1 MOFs were focused on carrying azobenzene and its derivatives as guests (Figure 4a).

There are several considerations to be reflected in Gen-1 MOFs such as compatibility between the framework's pore aperture and the size of the photoresponsive guest and a proper embedding procedure. Physical adsorption is widely applied to embed guest molecules inside the MOF, which is a simpler procedure to perform.[72] Hermann et al.[70] applied adsorption from a gas phase to incorporate azobenzene moieties into the pores of MOF-5, MIL-53 (Al), MIL-69 (Ga), and MIL-68 (In). They showed that *trans/cis* isomerization of AZB in the obtained host–guest systems was improved compared to that of the AZB in the solid state in all MOFs except MIL-53 (Al), where photoinduced isomerization was hindered by too high loading of AZB within the channels of MIL-53 and a subsequent lack of free volume. On the other hand, applying adsorption to embed photoswitches into the MOFs gives rise to the issue of guest stability as physically adsorbed molecules are easy to remove from pores during solvent washing or vacuum drying steps.[70] Gen-1 MOF photochromic properties are affected by the degree of guest loading, i.e., the packing of the guest molecules within the MOFs' pores. This parameter is analogous to grafting density in polymeric membranes in terms of its effect on the separation process: it also needs to be optimized as both too low as well as too high packing density would disturb material performance.[72] Lastly, a significant decrease of the MOFs' surface area is considered as a major limitation of this strategy.

3.4.2. Photoresponsive MOFs: Generation 2. 3.4.2.1. Generation 2 MOFs. Generation 2 (Gen-2) MOF chromophores are introduced into the MOF structure as a ligand side group (Figure 4b,c). While Gen-1 MOFs suffer from photoisomerization yield decrease due to the desorption of the guest chromophores, stronger attachment of chromophores to the framework is provided by covalent bonding in Gen-2 MOFs.[73] Moreover, chromophore distribution is more uniform as the position of the photoswitches in the MOF structure are determined. A ligand can be functionalized with photoresponsive units prior to MOF synthesis[74,75] or after it in a postsynthetic treatment.[76,77] The former approach is advantageous as the synthesis with premodified linkers is

https://doi.org/10.1021/acsapm.2c00090
ACS Appl. Polym. Mater. 2023, 5, 1−30

usually simpler to perform. Azobenzene, diarylethene, spiropyran, and viologen are the most reported chromophores to be attached to MOF ligands. In gas separation, Gen-2 MOFs are known to be functionalized with AZB or DAE chromophores. Let us first look on Gen-2 MOFs used as such (in powder form) and then continue with MOF-inserted MMMs.

Healey et al.[78] synthesized the photoresponsive MOF-808 (Zr) where spiropyran was covalently attached by a two-step postmodification process. As reported previously, each modification step lowered the material's specific surface area (SSA). However, CO_2 adsorption capacity in modified MOF-808-SP was significantly higher than that in the original material, which can be attributed to the strong interactions between CO_2 molecules and N-containing heterocycles or NO_2 groups in spiro moieties than between CO_2 and btc ligand (1,3,5-benzene tricarboxylate).

MIL-101-NH_2 was postsynthetically modified by treating evacuated MOFs with azo-dye solution in a microwave oven.[77] The effect of the degree of PSM on isomerization yield was studied by varying molar ratios between ligand (BDC-NH_2^{2-}) and the dye form 2:1 to 1:2, achieving the maximum functionalization with the latter ratio. Smaller linker densities resulted in more free space in the pores and less steric hindrance and therefore a more pronounced switching effect. Azo-MIL-101 tested for methane sorption increased CH_4 adsorption capacity upon irradiation with UV light. The photofatigue of the MOF, which appeared in incomplete *cis*−*trans* isomerization, was also reported.

Hindrance of photoswitches and overall MOF mobility are frequently occurring phenomena also reported for PCN-123, which are MOF-5 (Cu) prepared with an azo-containing linker.[79] Here, the 1 h UV irradiation caused CO_2 uptake decrease to 26.6%. Interestingly, the second measurement performed after some time revealed an even higher decrease to 53.9%. This delay may be caused by slow photoisomerization of the PCN-123 ligand, which was due to steric hindrance among azo moieties. The same PCN-123 MOF was chosen for modeling studies to reveal guest (CO_2 molecule)−host interactions in the MOF pore. As such, the decrease of CO_2 uptake was attributed to the stronger interactions between *trans*-azobenzene and CO_2 molecules and their preferential adsorption near the metal oxide carboxylate groups in the PCN-123 binding sites.[80] Following that, blocking of the strong adsorbing sites at the metal nodes by azobenzene molecules in a *cis*-configuration was proposed to cause a reversible decrease in CO_2 adsorption upon isomerization.[81]

MIL-53 (Al) and UiO-66 (Zr) visible-light-responsive MOFs were synthesized via introduction of fluorinated azobenzene moieties into their structure.[58] The same *ortho*-fluoroazobenzene linker but different inorganic secondary building units (SBUs) was used, which allowed the influence of MOF architecture on photoswitching and performance of the MOFs to be discussed. F-azo-MIL-53(Al) demonstrated significantly reduced isomerization efficiency due to the congestion of the azobenzene units, which further led to lower CO_2 adsorption capacity, whereas F-azo-UiO-66 (Zr) provided an efficient photoresponse.

The same DMOF-1 (Zn) functionalized with NO_2, NH_2, Br, and azo groups were produced in a one-pot solvothermal synthesis and applied for postcombustion CO_2 capture.[82] SSA of the materials decreased in the row: original DMOF-1 − NO_2-DMOF-1 − Br-DMOF-1 − NH_2-DMOF-1 − azo-DMOF-1. Interestingly, CO_2 adsorption capacity increased in the row: azo-DMOF-1 − DMOF-1 − Br-DMOF-1 − NH_2-DMOF-1 − NO_2-DMOF-1; i.e., even though SSA of NH_2 and NO_2 was lower, stronger interactions between molecules of N and CO_2 contributed to higher adsorption. Lower CO_2 uptake was expected in the case of azo-DMOF-1 due to the SSA values. However, the calculated heat of adsorption did not decrease; on the contrary, its value was even higher than those of NH_2/NO_2-functionalized MOFs. This reveals a more favorable Lewis acid−base-type interaction between CO_2 and azo moieties. Further tests on CO_2/N_2 (15:85 mixture) selectivity of the materials demonstrated the superior performance of azo-functionalized DMOF with a separation factor of 40, whereas separation factors achieved with NH_2-DMOF-1 and DMOF-1 were 25 and 15, respectively, and lower with other MOFs.

The performance of generation 2 MOFs may suffer from steric hindrance[83] of photoisomerization and suppression of the cycloreversion reaction due to the stabilization of an isomer upon incorporation into the MOF ligand.[84,85] Additionally, the above-mentioned issue on surface area decrease remains as the photoresponsive ligand side group may protrude into the framework's pore.[86,87] Reduced pore volume causes not only a decrease in gas adsorption capacity when MOFs are intended to be used for such applications but may also lead to hindered photoisomerization. Five MOF types containing different metals and the same switchable AzBIPY linker were synthesized in the work of Modrow et al.,[74] and only small changes were observed in the framework structure upon UV irradiation, which was ascribed to the limited porous space. Varying length of a linker was proposed as a possible strategy to overcome the issue.

3.4.2.2. Gen-2 MOF-MMMs. Work performed on the topic of preparation of MMMs with Gen-2 and Gen-3 MOFs as fillers was mostly performed by Prasetya et al. at Imperial College London. In his work, azobenzene photoswitches were introduced into DMOF[88] and UiO-66[89,90] frameworks that were incorporated as fillers in PIM-1 and Matrimid GS membranes. Results on the obtained SSA and pore volume of azo-DMOF-1 and azo-UiO-66 (with different azo loading investigated) MOFs in a powder form with corresponding CO_2 uptake under normal conditions and UV irradiation and CO_2/N_2 selectivity are summarized in Table 2. The aforementioned pattern on the decrease of MOF surface area and pore free volume with the increase of functionalization density and subsequent decrease of CO_2 uptake was observed for all reported MOFs. As an example, adding azo functionality in both UiO-66 and DMOF decreased SSA 2.6 times in both MOFs, but CO_2 uptake at 298 K by azo-DMOF-1 decreased 2.85 times, whereas it was only 1.05 times lower (i.e., almost not affected) for azo-UiO-66. This difference can be explained through different guest−host interactions involved. Small changes in azo-DMOF-1 were attributed to the lowest energetic site, where CO_2 is most favorably adsorbed. Regardless of the introduced functionality, this area, which is close to the metal site, remains undisturbed at relatively low pressure, hence, not causing significant changes in CO_2 uptake. At higher relative pressure (P/P_0), however, the changes become more pronounced, revealing a declining adsorption capacity of azo-DMOF toward CO_2 uptake. CO_2 adsorption at 298 K by nonirradiated azo-DMOF[88] and azo-UiO-66[90] (azo moiety in a *trans*-form) was 1.48 and 3.79 times higher than that for UV-exposed MOFs (azo moiety in a *cis*-form). The

https://doi.org/10.1021/acsapm.2c00090
ACS Appl. Polym. Mater. 2023, 5, 1−30

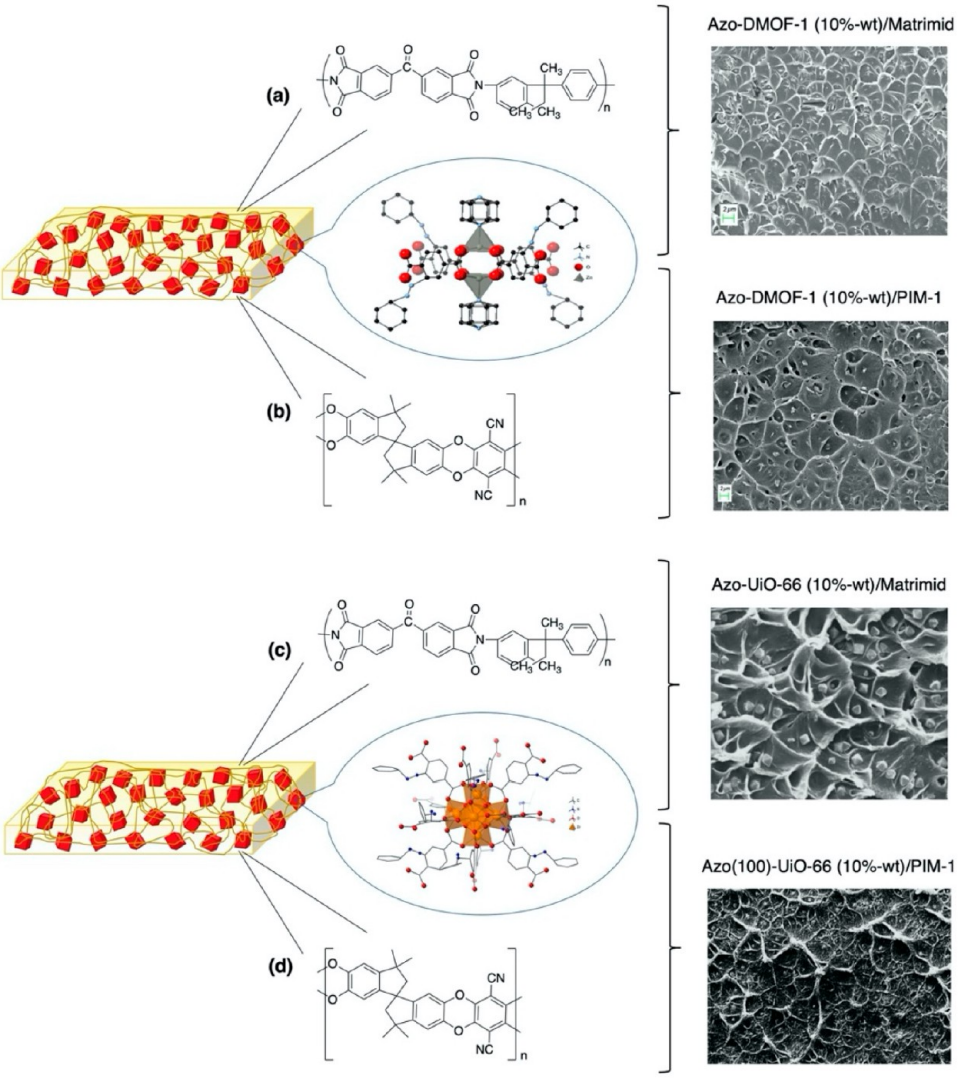

Figure 5. Gas separation MMMs with Gen-2 MOFs as fillers: azo-DMOF-Matrimid (a) and azo-DMOF-PIM (b). Reproduced in part from ref 88. Copyright 2018 American Chemical Society. Azo-UiO-66-Matrimid (c). Reprinted in part with permission from ref 89. Copyright 2018 The Royal Society of Chemistry. Azo-UiO-66-PIM (d). Reprinted in part with permission from ref 90. Copyright 2019 The Royal Society of Chemistry.

reason behind this phenomenon lies in azobenzene conformational changes from the *trans*-form to the *cis*-form and consequent changes in azobenzene–CO_2 interactions. Examined heat of adsorption that reflects the interaction between adsorbent and adsorbate for the UV-irradiated MOF samples was lower than that for the irradiated ones, which confirms less stronger affinity takes place.

CO_2 adsorption by various azobenzene-functionalized MOFs revealed that there are several distinguishing aspects: a decrease of the framework's pore volume, which causes a drop in CO_2 adsorption capacity and thus represents an overall drawback, and an increase of CO_2/N_2 selectivity, which is clearly beneficial for selective CO_2 capture. However, both aspects can become advantageous when applied to mixed-matrix membranes in CO_2 separation applications. Introducing highly porous materials into the membrane structure has a positive effect on overall gas permeability, i.e., for all gas mixture components. Here, the decreased pore volume does not have much effect on the process performance. At the same time, enhanced CO_2/N_2 selectivity, originated from the preferential interaction between azo functionalization and CO_2 molecules, continues to be an obvious advantage. For the photoresponsive property itself, this feature may find possible applications as molecular valves for adjusted gas flux or flammable gas mixture control.[85]

MMMs incorporated with either one of the above-mentioned MOFs (azo-DMOF and azo-UiO-66) were prepared by the doped film casted onto a Petri dish, and the membranes were formed in a solvent evaporation process. A linker was functionalized with azobenzene moieties prior to MOF synthesis. Matrimid and polymer of intrinsic microporosity (PIM-1) were used as the polymer that composes the membrane matrix giving four different MOF–polymer MMM types: azo-DMOF-Matrimid (Figure 5a), azo-DMOF-PIM (Figure 5b),[88] azo-UiO-66-Matrimid (Figure 5c),[89] and azo-UiO-66-PIM (Figure 5d).[90] To moderate morphology of the forming membranes, the solvent evaporation rate was adjusted by covering Petri dishes with aluminum foil. It has an effect of slowing the evaporation, causing tighter membranes to form and eliminating the temperature or humidity gradient in the air near the membrane surface, leading to a more homogeneous

https://doi.org/10.1021/acsapm.2c00090
ACS Appl. Polym. Mater. 2023, 5, 1–30

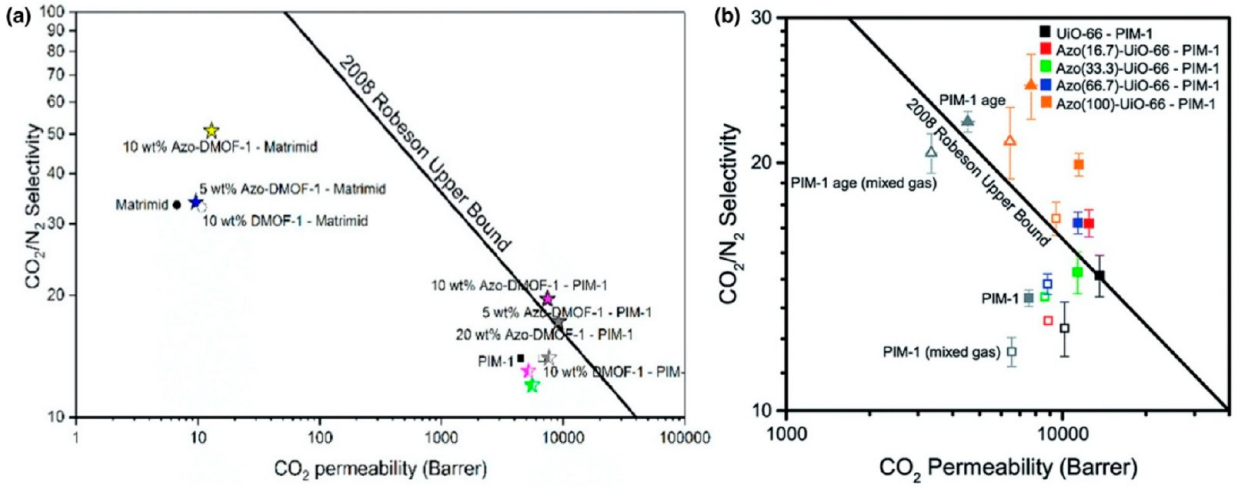

Figure 6. CO_2/N_2 separation performance of some of the synthesized Gen-2 and Gen-3 MOF-MMMs: Matrimid-azo-DMOF and PIM-azo-DMOF; filled symbols are for pure gas performance, half-filled symbols are for mixed gas (a). Reproduced from ref 88. Copyright 2018 American Chemical Society. PIM-azo(x)-UiO-66; square symbols are for pure gas performance, star-shaped symbols are for mixed gas (b). Reprinted with permission from ref 90. Copyright 2019 The Royal Society of Chemistry.

membrane structure. MOF loading was varied from 5 to 20 wt % of the polymer's weight.

The obtained MMMs were evaluated in terms of their CO_2 permeability and CO_2/N_2 selectivity in single-gas and equimolar mixture gas permeation experiments. The results are shown in Table 2. All four types of membranes—azo-DMOF-Matrimid, azo-DMOF-PIM, azo-UiO-66-Matrimid, and azo-UiO-66-PIM—have shown similar trends. For single-gas permeation measurements, introducing MOFs into the matrix, permeability of gases, both CO_2 and N_2, increases in Matrimid and PIM-1-based membranes as expected. Nevertheless, neither DMOF-1 nor UiO-66 (unmodified) affects the ideal selectivity parameter. This is a typical situation: the MOF filler causes a great positive effect on gas fluxes, while selectivity remains constant. However, that is not the case when azo-modified frameworks are applied: both gas permeability and CO_2/N_2 selectivity increased. Higher azo-MOF loadings made permselectivity changes more pronounced in most of the cases.

A similar situation was observed with equimolar gas mixture conducted with the PIM-azo-DMOF membranes.[88] The difference from the single-gas experiments was in the "rate" of permselectivity improvement: the achieved values exceeded the pristine PIM-membrane in a mixed-gas scenario but not the ones obtained with the same PIM-azo-DMOF membranes in single-gas tests. In the mixed-gas scenario, the decrease in CO_2 permeability was attributed to the competitive permeation with N_2. Additionally for mixture gases, azo-DMOF in MMMs has a stronger effect on the selectivity parameter than on permeability. The calculated diffusion coefficients for both gases increased due to the increased free volume through the polymer matrix, which once again confirms the reason behind the improved permeability, but have almost negligible impact on diffusion selectivity. Meanwhile, solubility coefficients decreased for CO_2 and N_2 due to the lower gas solubility in the filler materials than in polymers. Nevertheless, solubility selectivity increased due to the above-mentioned thermodynamically favorable interactions between azobenzene and CO_2 over N_2. That is the role of the azo functionality added to the DMOF filler that causes higher attraction of the MOF toward CO_2 via Lewis acid−base interactions. Additionally, the nitrogen-rich atmosphere in azobenzene groups makes the environment "nitrogen-phobic", which results in lower affinity between N_2 and azo-modified fillers.

The same patterns were revealed for the PIM-azo(X)-UiO-66 membranes applied for the mixed feed gas of CO_2/N_2 in a 15:85 ratio (simulated combustion gas composition at coal or natural gas power plants).[90] Namely, (a) lower permeability and selectivity in MMMs with all types of MOFs in the mixed-gas scenario are compared to the same membrane performance in the single-gas permeation, and (b) higher permselectivity occurs in MMMs with azo-MOFs against MMMs with unmodified fillers in mixed-gas tests. The reasons that caused these phenomena were once again attributed to the increased gas diffusivities due to the increased free volume into the membrane film caused by MOF introduction and thermodynamically favored interactions between azo groups and CO_2 molecules over N_2, which are because of more nitrogen-saturated atmosphere in azo moieties. In PIM-azo(X)-UiO-66, "X" stands for the percentage of azo-modified terephthalic acid linkers out of the full amount of linkers added (the rest was unmodified terephthalic acid). With increasing "X", i.e., the number of azo groups in the filler, gas permeability experienced a slight decrease as the free volume became partially occupied by introduced azo molecules. Along with this, a pronounced increase in selectivity is a clear advantage of having azo moieties in MMMs.

The permeability and selectivity of the discussed above MMMs are illustrated in Figure 6, where the data obtained with Gen-2 MMMs along with Gen-3 MMMs are shown. Figure 6 aims on illustrating in the form of Robeson diagrams the most promising results obtained so far with photoresponsive gas separation membranes with a polymeric matrix (mixed matrix, for these cases).

3.4.3. Photoresponsive MOFs: Generation 3. 3.4.3.1. Generation 3 MOFs. Generation 3 (Gen-3) MOFs contain photoresponsive units introduced into the MOF structure as a ligand backbone (Figure 4d,e). Incorporation of chromophores into the MOF skeleton is probably the most challenging approach due to the restrictions on isomer

https://doi.org/10.1021/acsapm.2c00090
ACS Appl. Polym. Mater. 2023, 5, 1−30

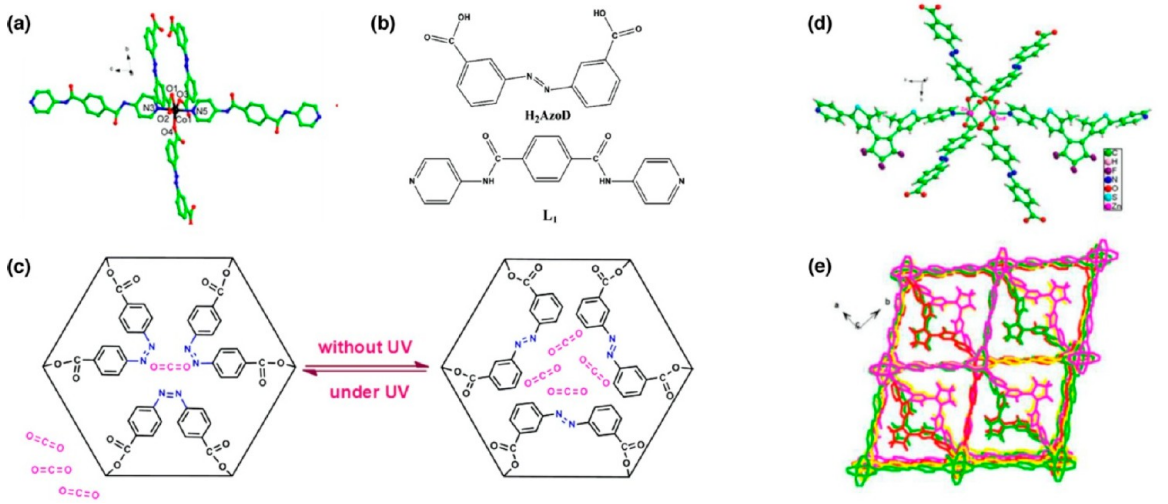

Figure 7. Schematic view of Gen-3 MOF unit structure. $Co_2L_2(AzoD)_2{\cdot}2DMF$: the simplest MBU (a), the ligands (b), and photoinduced structural changes in the MOF cage (c). Reprinted in part with permission from ref 96. Copyright 2016 Taylor & Francis. $Zn(AzDC)L_{0.5}{\cdot}(DMF)_{1.5}$: the paddle-wheel MBU (d) and the 3D framework (e). Reprinted in part with permission from ref 97. Copyright 2017 The Royal Society of Chemistry.

configurations as it affects MOF crystallinity and overall integrity.[86] For example, spiropyran[22] may have limits in being applied as a part of a backbone: the changes between geometry of isomers are quite large, which could either result in a hindrance of photoswitching or a framework degradation upon photoirradiation.[42] Thereupon, the Gen-3 MOF structure should be carefully considered prior to the synthesis. Nevertheless, there are studies that have reported successful preparation of Gen-3 MOFs with diarylethene[93,94] and azobenzene[95] derivatives inserted into ligands. To incorporate a photoswitch into a framework, the molecule can be modified with anchors that provide coordination with a metal cluster group.[42] As stated above, Gen-3 frameworks are of particular interest as their structure is directly affected by light irradiation, which results in significant transformations.[73] Another vital benefit of this strategy is preservation of the MOF surface area as there are no chromophore molecules inserted into the porous framework space.

Azobenzene-containing Gen-3 MOFs (Co) with a formula of $Co_2L_2(AzoD)_2{\cdot}2DMF$ were synthesized in a solvothermal reaction by Dang et al.[96] The architecture of the MOFs (the simplest metal building unit is depicted in Figure 7a) is interesting as it contains two types of ligands, H_2AzoD and L_1, for which the structure is given in Figure 7b, that are built along *b* and *c* axes, respectively. The adsorption capacities for CO_2 measured under the pressure of 1 bar were 19.4 and 13.7 cm^3/g at 273 and 298 K, respectively. Additionally, high selectivity over other gases (N_2, CO, and O_2) was due to stronger interactions between CO_2 and the MOFs. Irradiation of the MOFs with UV light transferred the energy to the azo bonds, causing conversion of *trans*-forms to *cis*-isomers. That resulted in reduction of the framework pore aperture (Figure 6c), where adsorbed CO_2 molecules were accommodated and triggered CO_2 release. Thus, CO_2 adsorption capacity of UV-exposed azo-MOFs is lower than that of the nonirradiated ones.

Fan et al.[97] reported a synthesized ECUT-30 MOF with a formula of $Zn(AzDC)L_{0.5}{\cdot}(DMF)_{1.5}$, for which the simplest metal building unit and 3D framework architecture are shown in Figure 7d,e, respectively. The ECUT-30 MOF is of particular interest as it contains two photoresponsive compounds: along with the relatively investigated azobenzene, diarylethene was also included in the framework structure. The azo units were carried by H_2AzDC (4,4-diazene-1,2-diyldibenzoate acid), which was also the ligand in the *b*-axis in the above-mentioned work of Dang et al.[96] The second ligand L_2 (4,4′-(4,4′-(perfluorocyclopent-1-ene-1,2-diyl)bis(5-methylthiophene-4,2-diyl))dipyridine) introduced diarylethene groups that are located along *a*-axis in ECUT-30. In the nonirradiated state, gas adsorption capacities for CO_2, C_2H_4, and C_2H_2 measured under the pressure of 1 bar were 29.8, 41.7, and 45.8 cm^3/g at 273 K and 19.6, 31.9, and 34.1 cm^3/g at 293 K, respectively. Calculated adsorption selectivities for C_2H_2/CO_2, C_2H_4/CO_2, and C_2H_2/C_2H_4 were in the range of 2.4−1.3, 2.8−1.7, and 0.8−0.7, respectively. As previously reported, UV light irradiation causes reduction in CO_2 adsorption capacity, which decreased to 28.6% in this study (measured at 1 bar, 293 K). Interestingly, the same conditions led to a 7.3% reduction in C_2H_2 uptake and 6.6% increase in C_2H_4 uptake, revealing the light modulation guest adsorption behavior in ECUT-30 MOFs. Consequently, adsorption selectivities for C_2H_2/CO_2 and C_2H_2/C_2H_4 increased to 50 and 108%, respectively, and decreased to 43.5% in the case of C_2H_4/CO_2, which illustrates a possibility for adsorption selectivity adjustment. The location of the adsorbed gas molecules in the framework was the main reason behind the observed light modulation guest adsorption behavior: the closer the distance between a molecule and a photoresponsive unit, the higher the changes in guest adsorption. The known strong interactions between CO_2 and azo groups determined CO_2 molecules were densely adsorbed at the corner of ECUT-30 supercages, close to the −N═N− bond in the AzDC ligand, i.e., close to the photoresponsive unit, whereas C_2H_2 and C_2H_4 were loosely located at the center of the channels. Even though ECUT-30 belongs to Gen-3 MOFs, no obvious movement of the MOF skeleton was observed after UV irradiation. Namely, regarding azo groups, no *cis*-adsorption bands appeared, and yet the *trans*-form showed a decrease in adsorption, which might be due to C−C−N bending movement of the $AzDC^{2-}$ ligand rather than *trans*−*cis*

https://doi.org/10.1021/acsapm.2c00090
ACS Appl. Polym. Mater. 2023, 5, 1−30

isomerization. For diarylethene, UV exposure resulted in the occurrence of only a partial ring-closing reaction.

The phenomenon of ligand restricted bending, i.e., inability of the ligand to undergo complete photoisomerization, was also discussed by Prasetya and Ladewig[98] for (azo-)JUC-62 (Cu) MOFs. The rigid JUC-62 framework restricted the ligand from complete transformation under UV light exposure, which determined the framework's fast relaxation back to the initial, nonirradiated state and complete restoration of initial CO_2 adsorption capacity once the UV irradiation stopped. This observation of fast back-relaxation then explains a good agreement between CO_2 uptake measured in static and dynamic irradiation conditions. As such, CO_2 adsorption capacities obtained at 1 bar with nonirradiated MOFs were 102 and 46 cm^3/g at 273 and 298 K, respectively, which then decrease to 52 (50% decrease) and 30 cm^3/g (34% decrease) under UV light irradiation. It is known that the adsorption capacity of a material toward gases decreases with increasing temperature, which was demonstrated in many of the above-mentioned works. Remarkably, the effect of heat transferred with UV light irradiation was placed into the spotlight in this work. Namely, about 7% out of the whole 50% decrease in CO_2 uptake at 273 K was attributed to the increased temperature due to the UV heat and not to the photoisomerization changes. This question is further discussed in section 4.

3.4.3.2. Gen-3 MOF-MMMs. Even though conceptually Gen-3 and Gen-2 MOFs are quite distinguishable, the preparation of MOF-MMMs and performance patterns remain similar. JUC-62 (Cu) and PCN-250 (Fe/Co) MOFs, for which the ligand is built of azobenzene tetracarboxylic acid H_4ABTC, were introduced as fillers into Matrimid membranes.[91] By definition, Gen-3 MOFs carry photoresponsive groups in their backbones, and thus the pores of frameworks remain empty, which is reflected in the SSA values that were 1020 and 1376 m^2/g, respectively. Incorporation of both MOFs into the membrane matrix resulted in increased gas permeability due to the additional pathways for gas molecules to be transported, increased CO_2/N_2 ideal selectivity due to the CO_2−azobenzene interactions and a nitrogen-phobic environment in the azobenzene moieties, and decreased CO_2 permeability under UV light irradiation compared to ambient conditions. The data are shown in Table 2. Interestingly, even though Gen-3 MOFs contain photoresponsive groups in their skeleton and thus are susceptible for high degree of switching (MOFs in their pristine conditions show ap to 50% decrease in CO_2 uptake once UV irradiated), the degree of photoinduced decrease in CO_2 permeability through MMMs was much lower (8.5% decrease maximum). The rigid structure of the Matrimid polymer was most probably a reason behind partially restrained ligand bending, which lessened the response to UV light exposure.

All of the above-mentioned MMMs contained Gen-2 or Gen-3 MOFs synthesized via a solvothermal route in autoclaves in the furnace. In the work of Xin et al.,[92] Co(AzDC) MOFs with an azobenzene-containing ligand (4,4′-azobenzene dicarboxylic acid, AzDC, as a linker) synthesized in a solvothermal reaction and in a microwave-assisted (MW) method was investigated as a filler in Matrimid (PI) MMMs. Application of these techniques resulted in MOFs with different size and morphology. As such, MOFs with bulk structure and the size of 10−20 μm were obtained in the solvothermal approach, whereas in the microwave method, spherical particles of 500 nm in size were formed. MW-fabricated spherical Co(AzDC) MOFs exhibited light-modulated adsorption of SO_2: under UV irradiation for 2 h, SO_2 uptake decreased to 4.3 and 15.2% at 273 and 295 K, respectively. However, after 10 h of contact, the reduction was already 18.9 and 31.0% at the same temperatures. Longer contact time resulted in a higher degree of saturation of frameworks' pores with SO_2, and overall adsorption capacities measured with and without UV irradiation increased as did the difference between them.

In MMM fabrication, apart from a possible better distribution of smaller spherical MW MOF particles within the doped polymer, smaller MOF aperture size is expected to enhance the sieving effect, which improves MMM selectivity. Matrimid (PI)-Co(AzDC) [MW] MMMs applied in a dry state demonstrated improvement in CO_2 permeability and CO_2/N_2 selectivity compared to that of neat PI at the MOF loadings up to 10 wt %, after which permselectivity decreased due to formation of unselective defects in the membrane matrix (Table 2). However, when used in a humidified state, CO_2 permeability was constantly increasing with higher MOF loadings, whereas CO_2/N_2 selectivity was still the highest at a filler content of 10 wt %. Overall permeability of the humidified membranes was about 10 times higher than those in the dried state, which is ascribed to swelling of a membrane caused by an increase in polymer chain spacing due to the uptake of water molecules. The proposed enhancement in the size-sieving effect of Co(AzDC) [MW] with an aperture size of 0.35 nm, suitable for transport of CO_2 molecules (0.33 nm) but hindering N_2 (3.64 nm) movement, as well as presence of CO_2-philic azo group in the MOF structure implied the improved selectivity in PI-Co(AzDC) [MW] membranes compared to that with the neat PI. PI-Co(AzDC) (10 wt %) light-modulated behavior was illustrated by a decrease in SO_2 permeability and SO_2/N_2 selectivity at 57% each (Table 2) upon UV light exposure compared with the data obtained in the ambient test conditions. The decrease in permeability was caused by the azo group presented into the MOFs' channels through which SO_2 transportation takes place. Once UV irradiated, the azo −N═N− bond absorbs energy causing its bending, and isomerization from *trans*-form to *cis*-form occurs, thus changing the channel structure to a more closed one. The permeability of N_2, however, did not experience significant changes (which was reflected in the improved SO_2/N_2 selectivity) due to its relatively large molecular size.

3.4.4. Photoresponsive MMMs with Other Fillers: COPs and GO. An azobenzene-based nanoporous covalent organic polymer, azo-COP-2, was investigated as a filler in Matrimid, PIM-1, and polysulphone (PS) gas separation MMMs.[99] Applying COPs could create the advantageous filler−matrix interactions as both are entirely built from organic materials. Azo-COP-2, synthesized from tetrakisnitrophenyl methane and *p*-phenylenediamine through a metal-catalyst-free method, was dispersed into the polymer solution of either one of the main matrix polymers, casted on a Petri dish, and subjected to slow solvent evaporation. The obtained membranes contained 5, 10, or 15 wt % of the filler. CO_2 adsorption capacities of pristine azo-COP-2 were 2.12 and 1.28 mmol/g and decreased to 22 and 16% under UV light irradiation at 273 and 298 K, respectively, which confirmed the photoresponsive behavior of the COPs. The reason behind these observations was the same as that described previously for the *cis* and *trans* differences in geometry and dipole moment. Permeability of all azo-COP-2-

https://doi.org/10.1021/acsapm.2c00090
ACS Appl. Polym. Mater. 2023, 5, 1−30

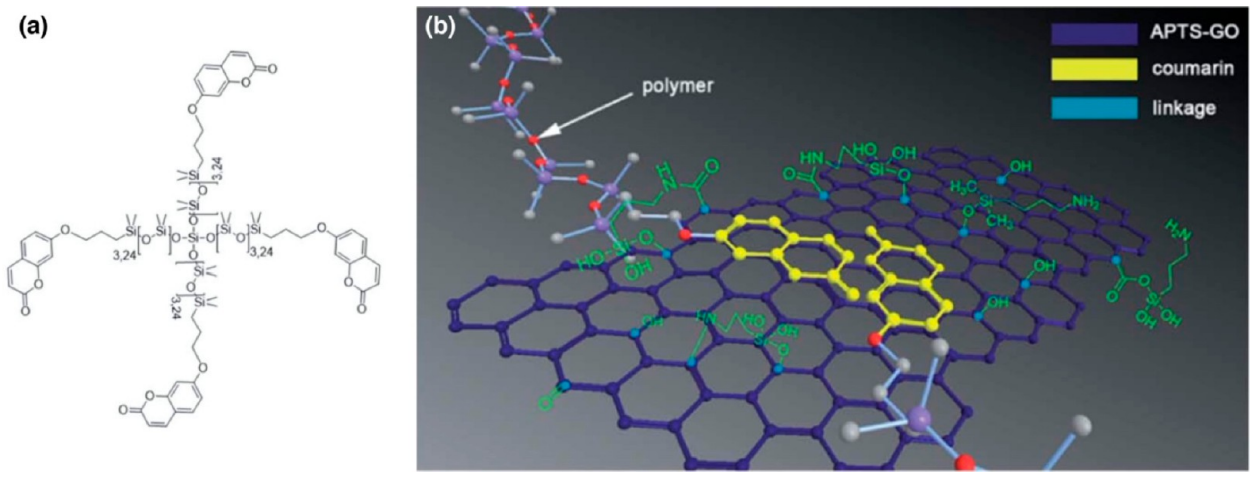

Figure 8. Chemical structure of the sPDMS (a) and its interactions with the APTS-GO surface (b). Reprinted with permission from ref 100. Copyright 2021 The Royal Society of Chemistry.

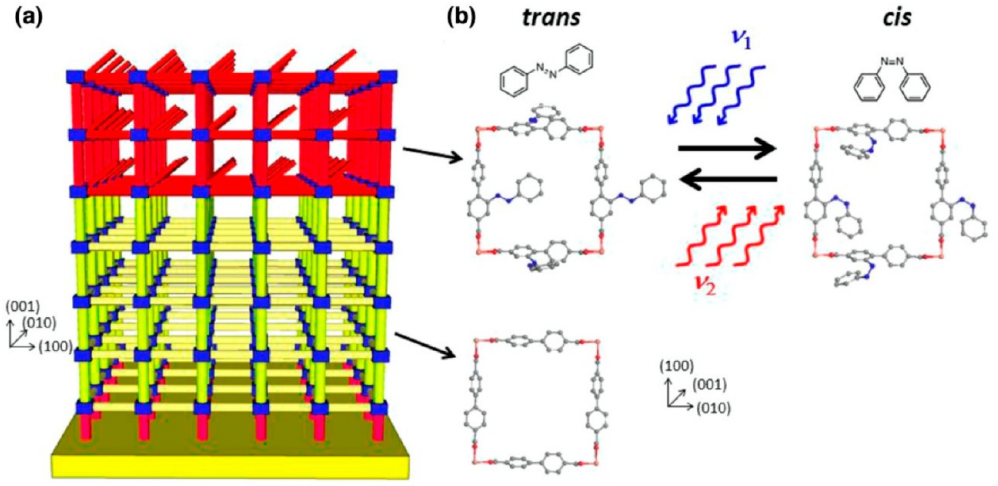

Figure 9. Structural drawing of heteroepitaxial two-component MOF: the photounactive $Cu_2(bpdc)_2(bipy)$ SURMOF (yellow) is grown on the pretreated gold substrate, and the photoresponsive $Cu_2(ab\text{-}bpdc)_2(bipy)$ SURMOF (red) containing photoswitchable azobenzene is grown on top (a). View of the pore window in the [001] direction (b). Reproduced from ref 103. Copyright 2014 American Chemical Society.

MMMs was higher than that of pure corresponding polymers and increased with higher particle loadings due to the increased free volume. The highest permeabilities for Matrimid, PS, and PIM-1 MMMs at 15 wt % azo-COP-2 were 27.1, 14.8, and 10500 Barrer, respectively. It corresponded to 171, 160, and 133% increases toward the neat Matrimid, PS, and PIM-1. The increase in particle loading had a positive effect on CO_2/N_2 selectivity; however, formation of defects such as unselective voids on the polymer−particle interface led to a decrease in the selectivity at higher loadings. The best improvement in selectivity was observed for 10 wt % azo-COP-2-Matrimid (26.3 against 23 in the neat Matrimid), 15 wt % azo-COP-2-PS (22.8 against 14), and 5 wt % azo-COP-2-PIM (16 against 14.3) membranes. The observed variation in selectivity coefficients was explained via the analyses of gas solubility and diffusivity coefficients in the presented MMMs, which was linked with the polymer−COP interactions. As such, the overall highest improvements demonstrated by COP−PS membranes were attributed to the enhanced hydrophobic interactions between azobenzene functionality and PS as both are inherently hydrophobic, as well as to the increased PS chain flexibility (lower T_g), which may contribute to better interactions with the introduced fillers.

Star-shaped poly(dimethylsiloxane), sPDMS, bearing coumarin photoresponsive units as terminal groups in its arm structure was blended with organosilane-modified graphene oxide (APTS-GO) nanosheets and spin-coated onto the polymeric support.[100] The structures of the sPDMS and APTS-GO-sPDMS interactions are shown in Figure 8. Applied irradiation at a 365 nm wavelength caused the dimerization of the coumarin moieties in sPDMS-24-APTS-GO (the loading of APTS-GO to sPDMS was 0.5 to 100; 24 stands for the number of Si−O repeating units in the sPDMS prearm), which resulted in formation of highly cross-linked polymeric networks with lower free volume and, hence, decreased permeation performance. As the cross-linking reaction at 365 nm changes the free volume and adsorption ability of the polymer, the gases, for which permeability is governed by both adsorption and diffusion—O_2 and CO_2—demonstrated the highest photoinduced permeance reduction, whereas those gases, which permeability relies on only one of the mentioned factors (H_2, N_2, and C_3H_8), showed lower changes. Under the 254 nm light exposure, the reverse reaction of cleavage of the

https://doi.org/10.1021/acsapm.2c00090
ACS Appl. Polym. Mater. 2023, 5, 1−30

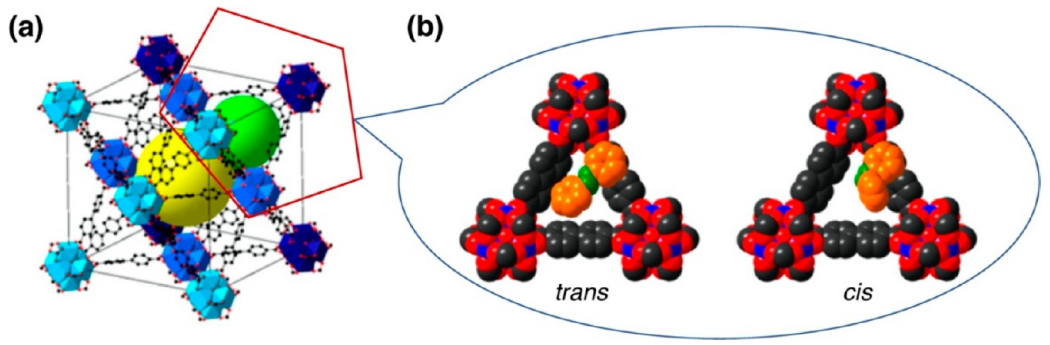

Figure 10. Crystal structure of the UiO-67 MOF composed from a two-cage structure: larger octahedron (inner cage space is shown in yellow) and smaller tetrahedron (inner cage space is shown in green) (a), and a sketch of the gate switching mechanism in the tetrahedral pore window of azo-UiO-67 (b). Reproduced from ref 104. Copyright 2017 American Chemical Society.

dimer bonds occurred with a consequent restoration of gas permeability but not to the exact initial values. Here, the largest increase was observed for the gases, for which permeability relies strongly on diffusion (H_2, N_2), whereas the increase for the solubility-driven permeance of O_2, CO_2, and C_3H_8 was much lower. The contribution of the APTS-GO filler increased the rate and degree of coumarin dimerization under 365 nm, which was due to the closer packing of coumarin molecules to each other once attached to the GO that assured the minimal distance between reactants required for the reaction to occur. The decrease in the rate and degree of cleavage reaction under 254 nm was attributed to the APTS-GO UV absorption at 240 nm, which reduced the UV energy available for the coumarin dimers.

3.5. Synthesis and Performance of MOF Thin Film Composite Membranes. There is a huge variety of inorganic gas separation membranes; however, the most interesting and developing inorganic membranes with a photoresponsive behavior are represented by the MOF thin film composite types. In these membranes, photoresponsive moieties are introduced into the structure of MOFs as described above (Gen-1 and Gen-2 MOFs) that are in situ deposited onto the top of the pretreated ceramic support solvothermally (Figure 2d) or via liquid-phase epitaxy (Figure 2e). The formed MOF thin film acts as the main separation layer. According to the reported technologies, the most advanced synthetic approach is presented by an epitaxial layer-by-layer (LBL) assembly to fabricate surface-anchored MOFs (SURMOF), where the obtained highly oriented MOF films had a controlled thickness.[101,102] Photoresponsive Gen-2 Cu_2(ab-bpdc)$_2$(bipy) SURMOFs with an azobenzene moiety as a ligand side group are schematically illustrated in Figure 9 (drawn in red).[103] In this work, a two-component SURMOF system was applied as a molecular container for capturing and holding butanediol and its phototriggered release. Specifically, photounactive Cu_2(bpdc)$_2$(bipy) SURMOF (bottom layer) deposited onto the modified gold support acted as container units. Photoresponsive Cu_2(ab-bpdc)$_2$(bipy) SURMOF (top layer), synthesized on the top of the photoinactive SURMOFs, was used as a photoswitchable valve that once closed to prevent of butanediol molecules from leaving the SURMOF pores and allowed the release of butanediol with an open-valve state.

3.5.1. Photoresponsive Gen-1 MOF Thin Film Composite Membranes. Synthesis of thin films of Gen-1 MOFs were reported in the works of Knebel et al.,[104] Fu et al.,[102] and Müller et al.[105] UiO-67 (Zr) frameworks were deposited onto a porous α-Al_2O_3 support by solvothermal growth, forming a 200 nm MOF thin film and substantially loaded with azobenzene molecules via adsorption of them from an acetone solution.[104] With completely loaded pores of the MOFs, photoswitching was greatly inhibited since dense packing of AZB left no free space for molecule transformations. Thereby, in situ thermally controlled desorption of AZB molecules from the thin film was applied, leaving the MOF film loaded with 19% of AZB instead of the initial 36.6%, showing the practical possibility to tailor the number of azo molecule guests into the framework for particular requirements. Single-gas permeances for the unmodified UiO-67 membrane were high due to the large pore cavities of the framework and increased with decreasing critical diameter of the gas molecules in the order of $C_3H_8 < C_2H_6 < CH_4 < CO_2 \approx N_2 < H_2$, and the ideal H_2 selectivities over other gas selectivities increased from 7.9 for H_2/N_2 to 18.3 for H_2/C_3H_8. Compared to UiO-67, the azo-UiO-67 membrane showed that permeances decreased for all gases due to the lower free pore space as partially occupied with AZB. Namely, H_2 permeance decreased from 10.20×10^{-7} to 4.41×10^{-7} in *trans*-azo-UiO-67 and to 5.10×10^{-7} $mol \cdot s^{-1} \cdot (m^2)^{-1} \cdot Pa^{-1}$ in *cis*-azo-UiO-67, whereas for CO_2, the decrease was from 1.17×10^{-7} to 0.30×10^{-7} and to 0.51×10^{-7} $mol \cdot s^{-1} \cdot (m^2)^{-1} \cdot Pa^{-1}$ in *trans*- and *cis*-azo-UiO-67, respectively. The H_2/CO_2 separation factor showed a good increase from 8.7 in unmodified MOF to 14.7 and 10.1 in *trans*- and *cis*-azo-UiO-67. Higher permeances with the membrane in the *cis*-form (obtained by UV irradiation with 365 nm light) compared to the *trans*-isomers (visible light of 455 nm wavelength) is attributed to the gating effect when changes in the length of the AZB isomers (5.5 Å for *cis*-form versus 9 Å for *trans*-form) causes opening/closing of the MOF pore's gate with aperture size of 8 Å (Figure 10). It is worth highlighting that, since in G-1 MOFs azobenzene photoswitches are guests in the framework pore, the *cis*-form provides higher gas fluxes, whereas in Gen-2 and Gen-3 MOFs, higher permeances are obtained with the *trans*-isomers. Therefore, the same *cis*−*trans* isomerization may cause polar effects depending on their structural position in MOFs or a membrane.

Apart from the solvothermal synthetic route, LBL assembly or liquid-phase epitaxial growth onto a functionalized substrate (the COOH-functionalized self-assembled monolayers (SAMs) of gold or the OH-terminated quartz glass) was reported to be suitable for Gen-1 MOF thin film preparation.[102] The HKUST (Cu) MOFs with encapsulated azobenzene molecules were assembled onto the substrates by its sequential immersion into the solution containing a metal

https://doi.org/10.1021/acsapm.2c00090
ACS Appl. Polym. Mater. 2023, 5, 1−30

precursor, ligand, and azobenzene. A total of 100 growth cycles left a highly oriented MOF film (SURMOF) with an ability for photoisomerization. Azo-HKUST (Cu) SURMOF, synthesized in a similar procedure, was tested for uptake of 1,4-butanediol.[105] The higher uptake was obtained with *cis*-azo-HKUST, which was attributed to the increase in the AZB dipole moment from 0 in *trans*-form to 3 in *cis*-form.

3.5.2. Photoresponsive Gen-2 MOF Thin Films. Liquid-phase epitaxial (LPE) growth is also a suitable procedure for Gen-2 MOF synthesis.[85,106,107] Two pillared-layer MOF structures—$Cu_2(BDC)_2(AzoBiPyB)$ and $Cu_2(DMTPDC)_2(AzoBiPyB)$—were synthesized using the linker molecules with azobenzene side groups by LPE (50 cycles) onto the functionalized gold substrate.[106] Azobenzene is connected by one phenyl ring to the framework, while the other phenyl ring points into the pore. An important difference in terms of photoisomerization is the distance between the azobenzene side groups, which is shorter in $Cu_2(BDC)_2(AzoBiPyB)$, preventing its azo molecules from being in contact with each other, whereas a mutual steric hindrance of the azobenzene side groups cannot be excluded in $Cu_2(BDC)_2(AzoBiPyB)$.

The $Cu_2(AzoBPDC)_2(AzoBiPyB)$ Gen-2 SURMOFs (LPE, 90 cycles) with three azobenzene moieties per unit cell were prepared onto functionalized gold thin films on silicon, quartz glass (for characterization), and asymmetric mesoporous α-Al_2O_3 support (for gas permeation tests).[85] The architecture of the MOFs is illustrated in Figure 11a. The azobenzene *cis*/*trans* isomer ratio in the thin film can be adjusted by controlling the illumination time and intensities of the light-emitting diode (LED) source with either 365 nm (UV, *trans*-to-*cis* transformation) or 455 nm (vis, back-isomerization) wavelength. The adjusted *cis*/*trans* ratio leads to adjusted gas separation factors that can be either increased or decreased. Namely, for the binary mixture of H_2/CO_2 (50%:50%, simulated precombustion mixture), the molecular separation factor might be increased from the minimum of 3.0 at the fully *trans* state (100% *trans*, 0% *cis*) to its maximum of 8.0 at the predominant *cis*-state (37% *trans*, 63% *cis*). For these transformations, about 5 h of irradiation was required in this study. With shorter exposure time, the separation factors between the values of 3.0 and 8.0 can be obtained. The higher H_2/CO_2 separation factor at the *cis*-state is attributed to the increase in the dipole moment of the *cis*-isomer compared to that of the *trans*, which causes higher attraction to the fairly strong quadrupole moment of CO_2 slowing its permeation, while H_2-azobenzene interactions are not affected by the *trans*−*cis* photoswitching. Separation factors of N_2/CO_2 (simulated postcombustion mixtures) were also changed from 5.5 to 8.5 when the amount of *trans*-isomers decreased from 100 to 37% *trans* upon UV 365 nm irradiation, which might be due to the preferential interactions between CO_2 and azo molecules that slows down its diffusion.

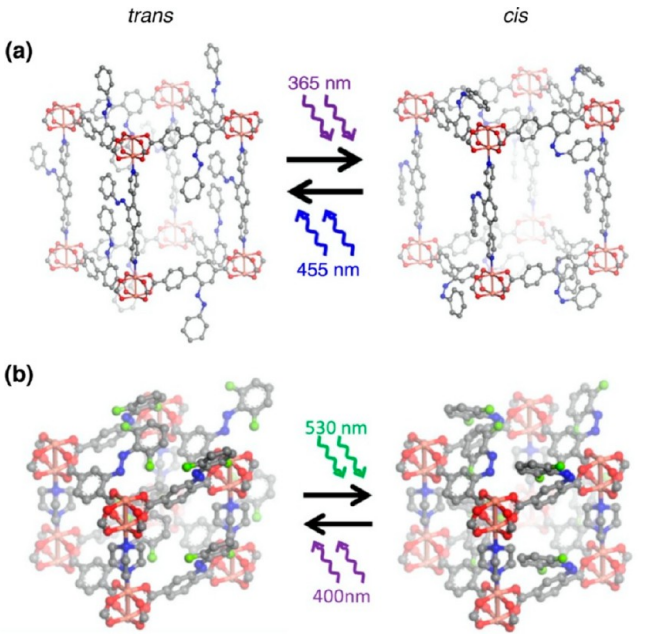

Figure 11. Structure of the $Cu_2(AzoBPDC)_2(AzoBiPyB)$ Gen-2 MOF in the *trans*- and *cis*-states (a). Reprinted with permission from ref 85. Copyright 2016 Springer Nature. The structure of the $Cu_2(F_2AzoBDC)_2(dabco)$ Gen-2 MOF in the *trans*- and *cis*-states (b). Reproduced from ref 108. Copyright 2021 American Chemical Society.

Thin films of $Cu_2(F_2AzoBDC)_2(dabco)$ Gen-2 SURMOFs (LPE) were synthesized with functionalized with fluoroazobenzene moieties to make the photoisomerization be governed by irradiation of visible light only (green and violet) instead of damaging UV spectra as well as to avoid ligand-to-metal charge transfer, which is excited by UV light in the Cu-paddlewheel MOF structures.[107] The MOF structure is given in Figure 11b.[108] The separation factors of H_2/C_2H_4 and H_2/C_3H_6 mixtures (simulated dehydrogenation of hydrocarbons) were increased by *trans*−*cis* isomerization triggered by 20 min irradiation with green light (530 nm) from 6.6 to 8.2 for the H_2/C_2H_4 and from 8.8 to 12.6 for the H_2/C_3H_6 mixtures. Back-isomerization and restoration of the initial separation factor values with a slight decrease can be achieved with irradiation by violet light at 400 nm. However, no significant effect of *trans*/*cis* isomerization was observed for the H_2/CO_2 mixture. That is because in the current study the $Cu_2(F_2AzoBDC)_2(dabco)$ MOF had smaller pore size, and hence, the steric effect of switching pore size (pore opening and closing) superimposed the polarity switching that was responsible for the polar observations reported previously by Wang et al.[85]

3.5.3. Other Photoresponsive Thin Films: Zeolites. Among inorganic membranes, not only MOF thin film but also zeolitic membranes are widely investigated for gas separation, and consequently, zeolites were investigated to host photoresponsive molecules. In the study of Weh et al.,[109] three zeolite-azobenzene membranes were synthesized by a two-step mechanism of seeding an α-Al_2O_3 support followed by hydrothermal synthesis of silicate-1 (MFI) or faujasite Na-X type (FAU) membranes (Figure 12). The loading of azobenzene molecules into the MFI and FAU were performed through gas-phase adsorption, leaving MFI-based membrane M-1 and FAU-based membranes M-2 (higher AZB content) and M-3 (lower AZB content). There is no classification for zeolite-photoswitch systems; however, the host−guest interactions refer to the Gen-1 photoresponsive framework materials.

AZB loading into zeolites' pores decreased the free volume in the membranes, resulting in a significant drop of permeabilities for all gases. Namely, CO_2 permeability decreased 113 and 4.5 times in M-1 and M-3 membranes, respectively. As the M-3 membrane was not fully loaded with

https://doi.org/10.1021/acsapm.2c00090
ACS Appl. Polym. Mater. 2023, 5, 1−30

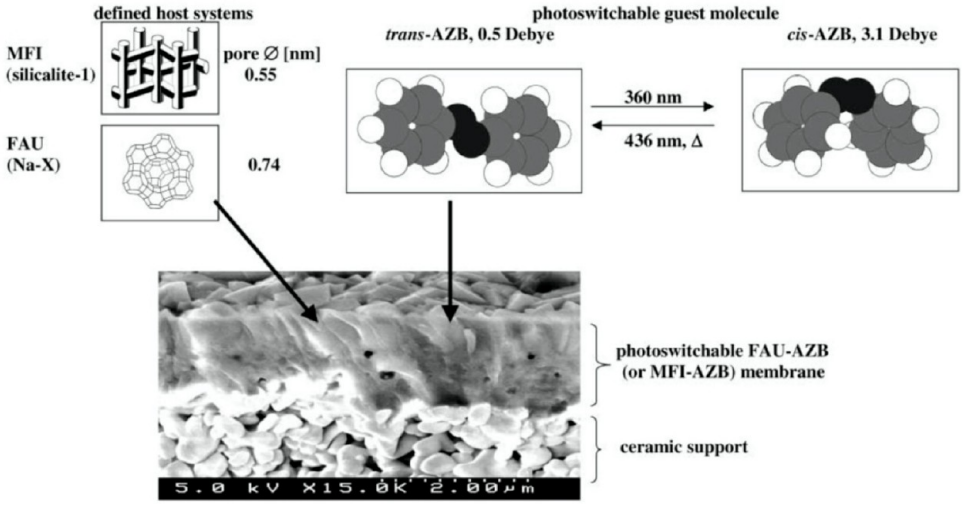

Figure 12. Schematic illustration and a microscopic image of the MFI-AZB and FAU-AZB membranes. Reprinted with permission from ref 109. Copyright 2002 Elsevier.

AZB, the observed permeability decrease was the smallest among all of the membranes, whereas the higher loaded M-2 exhibited the highest CO_2 decrease. In the MFI-based M-1 membrane, the obtained gas permeabilities decreased with increasing kinetic diameter of the molecules in both *trans*- and *cis*-configurations. However, this pattern was not observed in the FAU-based M-2 and M-3 because the effect of electrostatic forces, developed due to the presence of the heteropolar centers in the FAU-framework, overcame the dispersion forces. Further, transport of gas molecules was more inhibited in the *cis*-form membranes compared to their *trans*-configurations as *cis*-isomers are bulkier and have a higher polarity than the *trans* ones. Apart from H_2, for which *trans/cis* selectivity was almost not affected by the photoirradiation, the effect of *trans*−*cis* switching was the highest for the highest loaded M-2 membrane (10 AZB molecules per 0.74 nm unit cell) followed by M-1 (1−1.3 AZB molecule fer 0.55 nm unit cell) and M-3 (the number of AZB molecules per 0.74 nm unit cell is not given). The highest effect in M-3 was, however, not only due to the highest concentration of photoswitches but also due to their reallocation into the FAU framework from the supercages to the 12-ring entrance windows. Separation of CH_4/CO_2 and N_2/CO_2 equimolar gas mixtures, investigated with the M-3 membrane, revealed separation factors and permselectivities in the *trans*-form higher than those for the *cis*-state and for N_2/CO_2 than for CH_4/CO_2. The latter can be explained through the nonpolar nature of N_2 that allows the easier molecular transport, whereas the diffusion of quadrupolar CO_2 is inhibited when interacting with AZB. CH_4 may experience the inhibition if polarized by Na^+ from the FAU framework or *cis*-AZB.

3.6. Summary on Photoresponsive Gas Separation Membranes and Mechanisms. As it was shown in the given studies, the effect of photoresponsive moieties on gas separation performance depends on the photoresponsive mechanism involved, chromophore concentration, and, last but not least, the architecture of the material, i.e., the location if the chromophore in the polymer or MOF structure. As such, in polymeric membranes, introduction of azobenzene into the polymer backbone leads to an increase of gas permeance (compared to the neat polymer membrane) due to the rigidification of polymer chains due to the rigid −N═N− azo bond, which enables less efficient chain packing and, hence, a higher number of free gas pathways. AZB, covalently bonded to the polymer side chain, on the contrary, results in a permeance decrease as azo functionalization increases chain mobility, allowing them to be packed in a more space-efficient way, thus decreasing free volume within the membrane matrix. This effect becomes even more pronounced when AZB is physically blended with the main polymer. There, the permeance decrease is higher due to the occupation of polymer free volume by blended azobenzene molecules.

However, the increased chain rigidity and thus lower mobility of azo groups in a polymer backbone reduces the degree of photoresponse of the membrane, meaning that less pronounced changes in gas permeability and selectivity upon UV light irradiation (switching between *trans*- and *cis*-states) are obtained with azo moieties being introduced into the polymer main chain than when either added into the side chain or dispersed into the doped solution. Furthermore, comparing the photoresponsive behavior of side-chain-bonded and physically blended azobenzene-bearing membranes demonstrated that the blended films have a lower degree of photoresponse. The hindrance in photoisomerization might be caused by the unavailability of the buried membrane matrix photoswitches to light irradiation and partially by the occupation of membrane free volume by blended AZB molecules that enabled free geometrical transformations of chromophores.

Permeability of membranes in *trans*-form is higher than that in the *cis*-form as *cis*-isomers are bulkier due to its nonplanar, "curled", geometry, which increases polymer packing density and makes the gas pathways more tortoise shaped. In addition to this, the higher polarity of the *cis*-form reveals the possibility of additional dipole−dipole interactions between *cis*-molecules and some gases inhibiting their transport through the membrane.

In mixed-matrix membranes, introduction of a filler (usually represented by Gen-2 and Gen-3 MOFs) bearing photoresponsive groups increases gas permeability as the free volume within the membrane increases. The higher the filler concentration, the higher the permeance increases. However, within the same filler concentration, increased chromophore loading into the filler decreases gas permeance since the free

https://doi.org/10.1021/acsapm.2c00090
ACS Appl. Polym. Mater. 2023, 5, 1−30

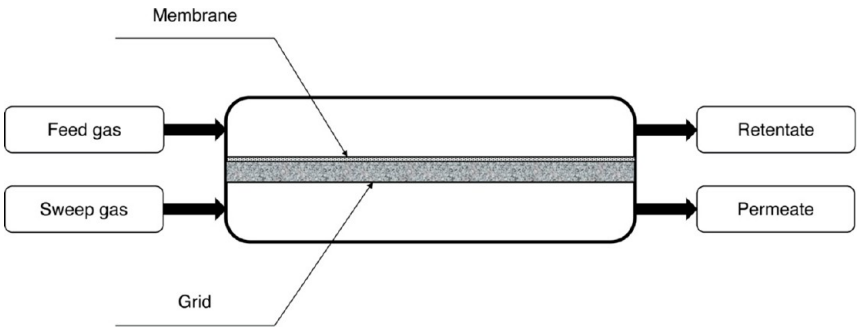

Figure 13. Schematic diagram of the Wicke-Kallenbach diffusion cell.

volume becomes occupied by photoswitches. Nevertheless, a significant increase in gas selectivity is seen as one of the main advantages of azo-functionalized fillers prior to unmodified ones. Specifically, the higher attraction between azobenzene groups and CO_2 molecules over other gases is due to the favorable Lewis acid−base-type interaction. Additionally, a "nitrogen-phobic" environment, developed due to the presence of azo moieties saturated with nitrogen, enhances CO_2/N_2 selectivity of the membranes. With the same polymeric matrix, performance of the membrane depends on the chosen MOF filler and its interaction with the main polymer, which determines membrane morphology. In the reviewed research, CO_2 permeabilities of Matrimid-based MMMs were more than 2 times higher with Gen-3 MOF fillers[91] than with Gen-2.[88,89] That can be explained to some extent via Gen-3 MOF architecture where the photoresponsive group is a part of the framework skeleton and, thus, does not occupy free volume in the MOF pores, whereas in Gen-2 frameworks, photoswitches are stated as ligand side groups that protrude into the MOF pores, decreasing membrane volume available for gas transport. However, an effect of the structure of each of the investigated MOFs—azo-DMOF-1, azo-UiO-66, JUC-62, and PCN-250—and its interaction with the main polymer and gaseous mixture on the membrane permeability and selectivity should be considered. As such, the phenomenon of ligand bending restriction, observed for Gen-3 MOFs, represents a challenge in photoresponsive MMM fabrication. That is when ligands in MOFs, introduced into MMMs, can undergo complete photoisomerization compared to the photoresponse given by the ligand in the same MOFs but being in the powdered form. The bending may be restrained upon the interactions between the filler and the rigid polymer matrix.

MOF thin film membranes, for which the separation layer is fully built of photoresponsive MOFs, higher gas permeabilities and the lowest separation factors were observed with Gen-2 MOFs in the *trans*-azobenzene state, whereas *cis*-isomers provided lower permeabilities and higher separation performance due to the above-mentioned differences between *trans*/*cis* geometry (open-channeled *trans* versus curled *cis*) and polarity (nonpolar *trans* versus polar *cis*). Interestingly, Gen-1 frameworks, i.e., MOFs with guest-encapsulated photoswitches, revealed the opposite relationships: under UV irradiation (AZB in the *cis*-state), the thin film membranes demonstrate higher permeability and lower separation factors. The reason was attributed to the planar changes in azobenzene molecules upon irradiation; however, this time the curled *cis*-structure facilitated gas transport through the membrane as more compact guest *cis*-isomers occupied lower space inside the framework pores than "unfolded" *trans*-azobenzenes.

4. TESTING APPROACHES FOR PHOTORESPONSIVE MEMBRANES

A highly effective gas permeation experiment setup is crucial to evaluate the permeability/selectivity ability of the membranes. Among them, the gas permeation cell is the core design component. The classic Wicke-Kallenbach (W-K) diffusion cell[110] consisted of two flows through compartments that are widely used for studying separation in porous membranes, as is schematically depicted in Figure 13. The measured gas flows steadily through the top plate, whereas a sweep gas runs through the bottom plate in such a way that the pressure in the two compartments, as well as the temperature, is exactly equal. The membrane is fixed in the bottom plate either with a locking O-ring made of silicon rubber or neoprene to prevent leakage.[111] The necessity for precise pressure control represents a major issue of the W-K cell, as even minor pressure instabilities will cause large measurement errors due to the intrusion of the viscous flow.[112]

To investigate the photoresponsive ability of the photoresponsive membranes in a gas separation process, researchers developed a unique permeation cell configured with an external light based on the basic theory of the W-K cell. An ideal gas permeation cell should meet the requirements of full and uniform membrane illumination (all areas of the membrane surface are subjected to the irradiation of the same light intensity) along with an absence of temperature fluctuations during the whole measurement no matter if the light is switched on or off. According to the light source differences and the cell structures, the photoresponsive permeation cell can be divided into three generations as discussed in the following sections.

4.1. Generation 1 Photoresponsive Permeation Cell.

The fixed position, wavelength, and light intensity of the light sources play an essential role in evaluating the photoresponsive ability of the gas separation membranes. The Gen-1 photoresponsive membrane cell was developed by Ladewig's group,[91] where a UV LED was used as the light source. The schematic view of the Gen-1 photoresponsive membrane cell, which is mainly composed of two components (in situ UV light and water loop system), is shown in Figure 14.

In this approach, a source of illumination emitting light of a fixed wavelength (λ = 365 nm, UV spectra) is mounted into the upper compartment cell and tightly sealed with epoxy resin. The presence of UV light inside the membrane cell supplies sufficient in situ irradiation to the whole membrane surface and allows dynamic investigation of the photoresponsive ability of the membrane by switching UV light on and off. Meanwhile, an adjustable DC power supply is connected to the light source to continuously supply the

https://doi.org/10.1021/acsapm.2c00090
ACS Appl. Polym. Mater. 2023, 5, 1−30

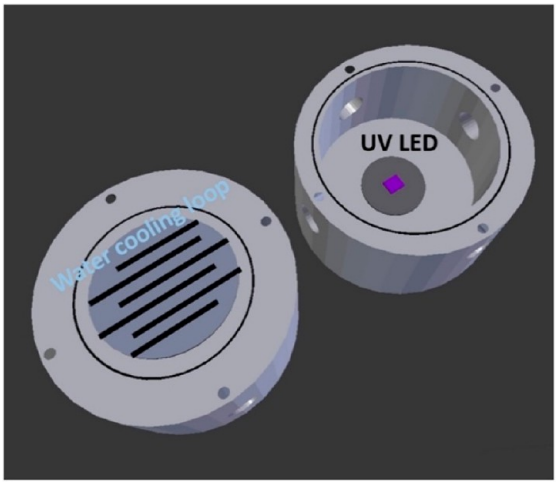

Figure 14. Schematic diagram of the Gen-1 photoresponsive membrane test cell. Reprinted with permission from ref 91. Copyright 2018 Springer Nature.

light of a specific intensity. Since the high-intensity UV light generates significant amount of heat while switched on, temperature increase inside membrane test cell takes place, which changes properties of the membrane and a feed gas and causes a large error being introduced into the measurements. Therefore, a water loop system was an important part to be designed and placed on the top of the membrane test cell to keep the temperature inside the cell at the set value during the experiments. Cold water is circulated through the cell top plate to remove the additional heat and to keep the temperature at a constant level while the LED is switched on; while the light is off, warm water could be used to maintain the same temperature as it was in the measurements under UV irradiation.[91] The water-cooling system, however, could take the heat away only partially, and thus, it is still challenging to keep the constant temperature during the whole measurement. Therefore, it was a pressing need to find a proper way to address the problem of the temperature increase in the top cell compartment caused by the light source.

4.2. Generation 2 Photoresponsive Permeation Cell. As mentioned above, using a LED powered by the DC source could generate some amount of heat once UV light is on and it would significantly affect the measurements. Therefore, an optical fiber-coupled LED was applied to the photoresponsive membrane cell.[104,107,113] Figure 15 illustrates the sketch of the Gen-2 photoresponsive membrane test cell, where a fiber-coupled, monochromatic high power Prismatix FC-5 LED is used for in situ irradiation of the membrane. The membrane test cell consists of two chambers designed based on the W-K principle but with the changes in the volume of the upper chamber (increased) and a use of optical-coupled LED mounted to the top of the upper chamber. Compared to the light source of Gen-1, the optical-coupled LED could produce an even cold light, which allows heat generation by the UV light illumination to be avoided. This way, in the Gen-2 light sources, the problem of heat generation was addressed and solved in the light source itself. However, some photoresponsive membranes could absorb the cold UV or vis light, and the absorbed energy then converts to heat, which again causes membrane heating and changes in gas transport.[98] In particular, the heat gained by membranes could confound the effects of the photoresponsive nature of the materials as gas

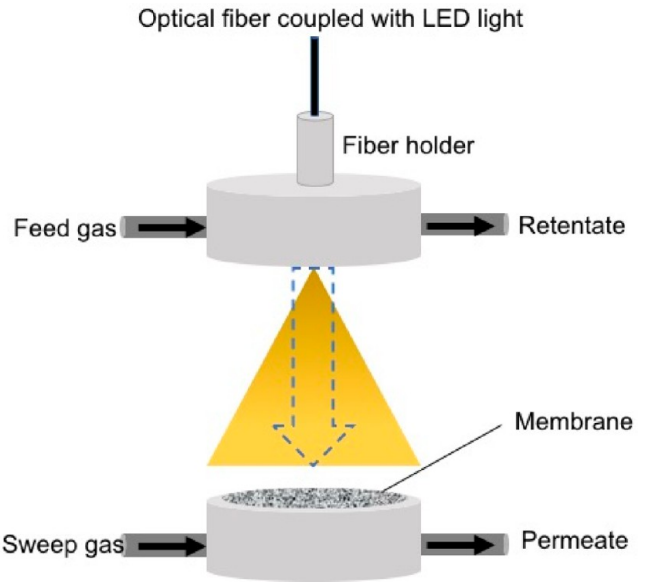

Figure 15. Sketch of Gen-2 photoswitchable membrane permeation test cell.

permeation can be changed by changing the temperature of the membrane. To address this issue, a Gen-3 photoresponsive permeation cell was developed.

4.3. Generation 3 Photoresponsive Permeation Cell. Combining the advantages of the Gen-1 and Gen-2 photoresponsive membrane cells, a remarkable multiple functional Gen-3 photoresponsive membrane test cell was designed by Ladewig's group and fabricated at the Institute of Microprocess Engineering (IMVT) at Karlsruhe Institute of Technology (KIT), Germany. In the scheme of Gen-3 presented in Figure 16, three different components, which could be tightly assembled via two O-rings, are illustrated. An optical fiber-coupled LED acts as the cold light source, and it is screwed to the top part of the upper cell. The distance from the end of the fiber to the top of the membrane must be carefully calculated according to the numerical aperture (NA) to ensure the light could illuminate the whole membrane area.

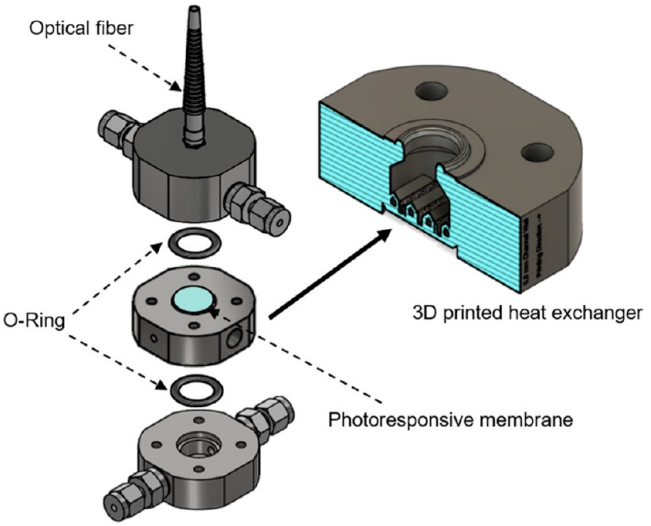

Figure 16. Schematic diagram of Gen-3 photoresponsive membrane test cell coupled with a 3D-printed microchanneled heat exchanger.

https://doi.org/10.1021/acsapm.2c00090
ACS Appl. Polym. Mater. 2023, 5, 1−30

To solve the problem of the heat gained via the absorption of light by the photoresponsive membranes, a novel 3D-printed metal heat exchanger (HE) was designed and printed by the selective laser melting printer in IMVT, KIT. The HE was introduced into the permeation cell as a middle part, where the surface containing a metal grid is facing up to allow the gas to diffuse through the grids, and the membrane is placed on the metal grid of the HE. As can be seen from the enlarged cross-sectional image of 3D-printed HE (Figure 15), the HE contains four inside microchannels, and the circulating cooling/heating water is pumped through them to maintain the constant temperature on the surface of the metal grid on which the membrane is placed. By coupling with the HE, the Gen-3 photoresponsive membrane cell could preclude the negative effects of the heat absorbed by membranes. Moreover, it can be applied to specified temperature conditions to evaluate gas separation performance of a temperature-responsive membrane by changing the circulating water temperature. Therefore, the Gen-3 photoresponsive membrane cell not only addresses the problem of Gen-1 and Gen-2 but also expands its application, providing the fundamental tool to reveal and determine the photoresponsive properties of the membranes.

4.4. Future Considerations: Large-Scale Photoresponsive Membrane Housing Modules. The next step after the laboratory experiments is pilot-scale membrane production and testing. In practice, gas separation membranes implemented on pilot or larger scales are produced in either one of the following modules depending on the ultimate application, i.e., the gaseous system to be processed. The most popular modules' choices are hollow fiber (HF), flat-sheet membrane stacks, and spiral-wound (SW) for polymeric membranes, and tubular/capillary for ceramic membranes, which is quite different from membrane coupons tested in the laboratory conditions. Even though SW and stacks are built up of flat membrane sheets, its fundamental difference is in the number of membranes rolled/stacked together and the fine space between them that did not allow to introduce a sufficient lighting to membrane surface. In this section, without providing a solution, we would like to highlight an importance of the question of proper module construction to keep membrane performance on a level closed to one demonstrated at the laboratory scale.

As stated above, a high number of tightly packed membrane sheets makes the membrane surface difficult to assess for emitted light. Even with the fiber-coupled LED source in situ generating the light of the set wavelength, only the upper membrane in the set would be fully irradiated. Thus, positioning of the light-emitting elements is questioned. An angle-positioned device might bring benefits related to better assessment of membranes; however, energy losses due to the dissipation are still expected to be significant. Furthermore, membrane housing is often made of steel, thus it is not transparent for neither of the light wavelengths, which poses a requirement for the light source to be coupled with the module. In addition, it puts some extra requirements on the air tightness of the construction in positions of the light source connection, so it would be hermetically sealed.

Those are the major questions to the developing modules for photoresponsive gas separation membranes raised at the present moment. Even when briefly mentioned, it becomes clear that the solution in order to work should be nontrivial, and principally novel approaches might be needed.

5. CONCLUSIONS AND OUTLOOK

This review attempts to highlight the very recent development of a series of photoresponsive membranes for gas separation along with the construction of photoresponsive permeation test modules. The available photoswitchable chemical groups, the membrane synthesis approaches, and the involved photoresponsive mechanisms were reviewed in detail. Further, the gas separation performance of photoresponsive organic (polymeric), inorganic (metal−organic framework, MOF, thin films), and organic−inorganic composite (MOF-based mixed matrix membranes) membranes is thoughtfully discussed. Since a majority of the studies were dedicated to the MMMs with photoresponsive MOFs as fillers and photoresponsive MOF thin films, a special attention in this review was brought to the development of photoresponsive properties in MOFs, which are then classified into three generations based on the position of the photoswitches in the framework structure.

To maintain the temperature constant when exposed to light irradiation and to overcome the issues of membrane heating by absorption of light, the novel architecture for the photoresponsive membrane permeation module was brought forward. There, the 3D-printed microchannel heat exchanger fabricated at the Karlsruhe Institute of Technology was applied in the photoresponsive gas separation measurements to keep the temperature unchanged, realizing an accurate evaluation of the photoresponsive ability of membranes. Moreover, the developed module could find a broader application than in the gas separation field. As such, the module—the heat exchanger and the optical fiber LED source—could be connected to the liquid permeation cell and thus be tested for photoresponsive membranes applied for water purification and liquid separation as well as drug release systems.

The future directions of photoresponsive gas separation are to develop photoresponsive materials and investigate their interaction mechanisms. Combining the high structural ordering of the SURMOF and high yield of photoresponse of Gen-3, it could be promising to synthesize Gen-3 SURMOF thin films to eliminate of hindrance of chromophore mobility as observed in Gen-3 MOF-MMMs. Regarding the photoresponsive units, studies could be expanded to molecules other that azobenzene and its derivatives that have been the focus in photoresponsive gas separation membranes so far due to the beneficial CO_2−azobenzene interactions. Nevertheless, more detailed investigation on the potential of diarylethene or spiropyran and other, not previously applied, chromophores will bring a better understanding of photoresponsive membrane systems.

It should be noted that for photoresponsive materials the future application is not limited by the gas separation field. Photoresponsive membranes are currently studied for biomedical applications such as drug delivery systems and selective drug release. For drug release applications, both reversible and irreversible chromophores could be used. There, photoinduced transformations in chromophores trigger collapse of the polymeric coverage of a medicine with its subsequent release. Other application areas are liquid separation and purification including water treatment, where geometrical light-triggered changes of photoresponsive units in the membrane structure could be applied for fine-tuning of membrane pore size, thus regulating membrane flux and molecular weight cutoff, MWCO, based selectivity (size exclusion). Moreover, charge-exclusion-based selectivity

https://doi.org/10.1021/acsapm.2c00090
ACS Appl. Polym. Mater. 2023, 5, 1−30

might be enhanced upon occurring transformations in photoswitch properties. Producing different types of sensors and selective gating systems, such as liquid valves discussed in this review, represents an interesting direction for further studies. In addition, photoresponsive materials, especially based on liquid-crystalline polymers, represent a promising topic of research for optical devices and in soft robotics. There, an ability of photoresponsive polymers to undergo a variety of geometrical transformations such as bending is used to produce mechanical movement of the nanorobotic machines.

Future research should not be exclusively focused on developing brand new photoresponsive materials but on improvement of the ones already investigated. Therefore, studies on overcoming the limitations related to the degradation of photoresponsive units causing photofatigue of the membrane are necessary. Furthermore, modification of photochromes in a way to switch the operating light wavelength to the visible spectra range without a decrease in membrane performance would be of great interest as it eliminates the damaging effects of UV light and makes the separation process less energy demanding.

■ ASSOCIATED CONTENT

Special Issue Paper

This paper was intended for the Polymer Membranes for Precision Separations special issue [*ACS Polym. Mater.***2022**, *4* (11)].

■ AUTHOR INFORMATION

Corresponding Author

Jinju Zhang − *Institute for Micro Process Engineering (IMVT), Department of Chemical and Process Engineering, Karlsruhe Institute of Technology, Karlsruhe 76344, Germany;* orcid.org/0000-0002-4276-6958; Email: jinju.zhang2@kit.edu

Authors

Anastasiia Gafiullina − *Department of Separation Science, LUT School of Engineering Science, Lappeenranta-Lahti University of Technology, Lappeenranta FI-53850, Finland;* Present Address: University of Luxembourg, Esch-surAlzette L-4365, Luxembourg

Bradley P. Ladewig − *University of Luxembourg, Esch-sur-Alzette L-4365, Luxembourg;* orcid.org/0000-0002-2135-1913

Complete contact information is available at: https://pubs.acs.org/10.1021/acsapm.2c00090

Author Contributions

The manuscript was written through contributions of all authors. Idea conceptualization and discussion of the manuscript: B.P.L., J.Zh., and A.G. Writing of the original draft: A.G. and J.Zh. Reviewing and editing: J.Zh. and B.P.L. All authors have given approval to the final version of the manuscript.

Notes

The authors declare no competing financial interest.

■ ABBREVIATIONS

APTS or APTES,(3-aminopropyl)triethoxysilane, a class of organizilanes; APTS-GO,organosilane-modified graphene oxide; ATRP,atom-transfer radical polymerization; AZB,azobenzene; azo- (as prefix),indicates that azo-bearing units (azobenzene or other polymers of the azo group) were introduced into the material; azo-PI,azo-PI membrane with azobenzene introduced into the backbone of polyimide (PI); zzoPMD,PMD77 with introduced into the side chain azobenzene; BET SA,surface area calculated with the Brunauer−Emmett−Teller method; COP,covalent organic polymer; DAE,diarylethene; DAE^{O},the open form of diarylethene; F-azo-UiO-66,metal−organic frameworks of the UiO-66 type with fluorinated azobenzene moieties introduced into the framework structure; FAU,faujasite Na-X; M-2,FAU (faujasite) Na-X type membrane with higher AZB content (zeolitic membrane); M-3,FAU (faujasite) Na-X type membrane with lower AZB content (zeolitic membrane); Gen,generation (for materials and equipment units); GS,gas separation; H_2AzDC,4,4-diazene-1,2-diyldibenzoate acid; H_4ABTC,azobenzene tetracarboxylic acid; HE,heat exchanger; L_2,4,4′-(4,4′-(perfluorocyclopent-1-ene-1,2-diyl)bis(5-methylthiophene-4,2-diyl))dipyridine); LED,light-emitting diode; LPE,liquid-phase epitaxial; MFI,silicate-1; M-1,MFI (silicate-1) type membrane (zeolitic membrane); MC,merocyanine; MMMs,mixed-matrix membranes; MOFs,metal−organic frameworks

MOF families and types:

DMOF, DABCO, (1,4-diazabicyclo[2.2.2]octane), or triethylenediamine, TEDA) MOF; HKUST, Hong Kong University of Science and Technology, where these MOFs were first synthesized; MIL-53, MIL-68, MIL-69, MIL-101, MIL stands for Materials of Institute Lavoisier, where these MOFs were first synthesized; MOF-5, MOF-808, metal−organic framework PCN-123, PCN-250; PCN stands for porous coordination network; UiO-66, UiO-67, University of Oslo, where these MOFs were first synthesized; MW, microwave; NA, numerical aperture; NDI, naphthalenediimide; NPs, nanoparticles; PAA, poly(acrylic acid); PAA-*g*-PP, poly(acrylic acid) grafted polypropylene membrane; PI, polyimide; PIM, polymer of intrinsic microporosity; PMA, polymethacrylate; PMAZB, polymethacrylate membranes carrying azobenzene units in the polymer side chain; PMD77, random copolymer of methyl methacrylate and 2-{ethyl-[4-(4-nitrophenylazo)phenyl]-amino}ethyl methacrylate); PMMA, poly(methyl methacrylate); PMMA/AZB, polymethacrylate membranes carrying physically blended azobenzene units; PP, polypropylene; PS, polysulfone; PSM, postsynthetic modification; redox potential, reduction−oxidation potential; SA, surface area; SAM, self-assembled monolayer; SBU, secondary building unit; SP, spiropyran; sPDMS, star-shaped poly(dimethylsiloxane); SS, stainless steel; SSA, specific surface area; SURMOF, surface-modified (or surface-anchored) metal−organic frameworks; UF, ultrafiltration; UV, ultraviolet; vis, visible; W-K cell, Wicke-Kallenbach diffusion cell

■ REFERENCES

(1) Aguilar, M. R.; Román, J. S.*Smart Polymers and Their Applications*, 2nd ed.; Elsevier, 2019.

(2) Weh, K.; Noack, M.; Ruhmann, R.; Hoffmann, K.; Toussaint, P.; Caro, J. Modification of the Transport Properties of a Polymethacrylate-Azobenzene Membrane by Photochemical Switching. *Chem. Eng. Technol.* **1998**, *21* (5), 408−412.

(3) Darvishmanesh, S.; Qian, X.; Wickramasinghe, S. R. Responsive membranes for advanced separations. *Curr. Opin. Chem. Eng.* **2015**, *8*, 98−104.

(4) Purkait, M. K.; Sinha, M. K.; Mondal, P.; Singh, R.Photoresponsive Membranes. *Interface Science and Technology*; Elsevier, 2018; Vol. 25, pp 115−144.

(5) Bhattacharyya, D.; Schäfer, T.*Responsive Membrane and Materials*; Wiley, 2013.
(6) Gelebart, A. H.; McBride, M.; Schenning, A. P. H. J.; Bowman, C. N.; Broer, D. J. Photoresponsive Fiber Array: Toward Mimicking the Collective Motion of Cilia for Transport Applications. *Adv. Funct. Mater.* **2016**, *26* (29), 5322−5327.
(7) Stumpel, J. E.; Broer, D. J.; Schenning, A. P. H. J. Stimuli-responsive photonic polymer coatings. *Chem. Commun.* **2014**, *50*, 15839−15848.
(8) Wagner, N.; Theato, P. Light-induced wettability changes on polymer surfaces. *Polymer* **2014**, *55* (16), 3436−3453.
(9) Zhao, Y. Photocontrollable block copolymer micelles: what can we control? *J. Mater. Chem.* **2009**, *19* (28), 4887−4895.
(10) Pantuso, E.; De Filpo, G.; Nicoletta, F. P. Light-Responsive Polymer Membranes. *Adv. Opt. Mater.* **2019**, *7* (16), 1900252.
(11) Danowski, W.; van Leeuwen, T.; Browne, W. R.; Feringa, B. L. Photoresponsive porous materials. *Nanoscale Adv.* **2021**, *3*, 24−40.
(12) Irie, M.; Fukaminato, T.; Matsuda, K.; Kobatake, S. Photochromism of Diarylethene Molecules and Crystals: Memories, Switches, and Actuators. *Chem. Rev.* **2014**, *114* (24), 12174−12277.
(13) Yokoyama, Y. Fulgides for Memories and Switches. *Chem. Rev.* **2000**, *100* (5), 1717−1740.
(14) Kumar, G. S.; Neckers, D. Photochemistry of Azobenzene-Containing Polymers. *Chem. Rev.* **1989**, *89* (8), 1915−1925.
(15) Irie, M.; Kunwatchakun, D. Reversible Photostimulated Dilation of Polyacryl-amide Gels Having Triphenylmethane Leuco Derivatives. *Macromolecules* **1986**, *19* (10), 2476−2480.
(16) Wang, X.*Azo Polymers: Synthesis, Functions and Applications*; Springer, 2017.
(17) Rau, H.Photoisomerization of Azobenzenes. *Photochemistry and Photophysics*; CRC Press, 1990; Vol. *2*, pp 119−141.
(18) Rau, H.Azo Compounds. *Photochromism: Molecules and Systems*; Elsevier, 2003; pp 165−192.
(19) Ercole, F.; Davis, T. P.; Evans, R. A. Photo-responsive Systems and Biomaterials: Photochromic Polymers, Light-Triggered Self-Assembly, Surface Modification, Fluorescence Modulation and Beyond. *Polym. Chem.* **2010**, *1*, 37−54.
(20) Hunger, K.; Mischke, P.; Rieper, W.; Raue, R.Azo Dyes. *Ullmann's Encyclopedia of Industrial Chemistry*, 5th ed.; Wiley-VCH: Weinheim, Germany, 1985; Vol. *A3*, pp 245−324.
(21) Berkovic, G.; Krongauz, V.; Weiss, V. Spiropyrans and Spirooxazines for Memories and Switches. *Chem. Rev.* **2000**, *100*, 1741−1754.
(22) Klajn, R. Spiropyran-Based Dynamic Materials. *Chem. Soc. Rev.* **2014**, *43*, 148−184.
(23) Fagan, A.; Bartkowski, M.; Giordani, S. Spiropyran-Based Drug Delivery Systems. *Front. Chem.* **2021**, *9*, 612.
(24) Eilmes, A. Spiropyran to Merocyanine Conversion: Explicit versus Implicit Solent Modeling. *Phys. Chem. A* **2013**, *117* (12), 2629−2635.
(25) Wang, L.; Li, Q. Photochromism into Nanosystems: towards Lighting up the Future Nanoworld. *Chem. Soc. Rev.* **2018**, *47* (3), 1044−1097.
(26) Hammarson, M.; Nilsson, J. R.; Li, S.; Beke-Somfai, T.; Andréasson, J. Characterization of the Thermal and Photoinduced Reactions of Photochromic Spiropyrans in Aqueous Solution. *J. Phys. Chem. B* **2013**, *117*, 13561−13571.
(27) Berton, C.; Busiello, D. M.; Zamuner, S.; Solari, E.; Scopelliti, R.; Fadaei-Tirani, F.; Severin, K.; Pezzato, C. Thermodynamics and Kinetics of Protonated Merocyanine Photoacids in Water. *Chem. Sci.* **2020**, *11*, 8457−8468.
(28) Radu, A.; Byrne, R.; Alhashimy, N.; Fusaro, M.; Scarmagnani, S.; Diamond, D. Spiropyran-based Reversible, Light-Modulated Sensing with Reduced Photofatigue. *J. Photochem. Photobiol. A: Chem.* **2009**, *206*, 109−115.
(29) Hanazawa, M.; Sumiya, R.; Horikawa, Y.; Irie, M. J. Thermally irreversible photochromic systems. Reversible photocyclization of 1,2-bis (2-methylbenzo[*b*]thiophen-3-yl)perfluorocyclocoalkene derivatives. *Chem. Soc., Chem. Commun.* **1992**, *3*, 206−207.
(30) Fukaminato, T.; Hirose, T.; Doi, T.; Hazama, M.; Matsuda, K.; Irie, M. Molecular Design Strategy toward Diarylethenes that Photoswitch with Visible Light. *J. Am. Chem. Soc.* **2014**, *136* (49), 17145−17154.
(31) Maeda, S.Spirooxazines. *Organic Photochromic and Thermochromic Compounds*; Plenum Publishing, 1999; Vol. *1*, p 85.
(32) Chu, N. Y. C. Photochromism of spiroindolinonaphthoxazine. I. Photophysical properties. *Can. J. Chem.* **1983**, *61* (2), 300−305.
(33) Nicoletta, F. P.; Cupelli, D.; Formoso, P.; De Filpo, G.; Colella, V.; Gugliuzza, A. Light Responsive Polymer Membranes: A Review. *Membranes* **2012**, *2*, 134−197.
(34) Bhosale, S. V.; Jani, C. H.; Langford, S. J. Chemistry of Naphthalene Diimides. *Chem. Soc. Rev.* **2008**, *37* (2), 331−342.
(35) Monk, P. M. S.*The Viologens: Physicochemical Properties, Synthesis and Applications of the Salts of 4,4′-Bipyridine*; Wiley, 1998.
(36) Cardenas-Daw, C.; Kroeger, A.; Schaertl, W.; Froimowicz, P.; Landfester, K. Reversible Photocycloadditions, a Powerful Tool for Tailoring (Nano)Materials. *Macromol. Chem. Phys.* **2012**, *213* (2), 144−156.
(37) O'Donnell, M. Photo-Dimerization of Solid Anthracene. *Nature* **1968**, *218*, 460−461.
(38) Tyer, N. W.; Becker, R. S. Photochromic Spiropyrans. I. Absorption Spectra and Evaluation of the π-electron Orthogonality of the Constituent Halves. *J. Am. Chem. Soc.* **1970**, *92*, 1289−1294.
(39) Cao, Z.; Wang, G.; Chen, Y.; Liang, F.; Yang, Z. Light-Triggered Responsive Janus Composite Nanosheets. *Macromolecules* **2015**, *48* (19), 7256−7261.
(40) Vlassiouk, I.; Park, C.-D.; Vail, S. A.; Gust, D.; Smirnov, S. Control of Nanopore Wetting by a Photochromic Spiropyran: A Light-Controlled Valve and Electrical Switch. *Nano Lett.* **2006**, *6*, 1013−1017.
(41) Pimienta, V.; Lavabre, D.; Levy, G.; Samat, A.; Guglielmetti, R.; Micheau, J. C. Kinetic Analysis of Photochromic Systems under Continuous Irradiation. Application to Spiropyrans. *J. Phys. Chem.* **1996**, *100*, 4485−4490.
(42) Rice, A. M.; Martin, C. R.; Galitskiy, V. A.; Berseneva, A. A.; Leith, G. A.; Shustova, N. B. Photophysics Modulation in Photoswitchable Metal-organic Frameworks. *Chem. Rev.* **2020**, *120* (16), 8790−8813.
(43) Weston, C. E.; Richardson, R. D.; Haycock, P. R.; White, A. J.; Fuchter, M. J. Arylazopyrazoles: Azoheteroarene Photoswitches Offering Quantitative Isomerization and Long Thermal Half-Lives. *J. Am. Chem. Soc.* **2014**, *136* (34), 11878−11881.
(44) Van Gembert, B.Benzo and Napthopyrans (Chromenes). *Organic Photochromic and Thermochromic Compounds*; Plenum Publishing, 1999; Vol. *1*, p 111.
(45) Jeong, Y.-C.; Yang, S. I.; Kim, E.; Ahn, K.-H. Development of highly fluorescent photochromic material with high fatigue resistance. *Tetrahedron* **2006**, *62* (25), 5855−5861.
(46) Jeong, Y.-C.; Park, D. G.; Lee, I. S.; Yang, S. I.; Ahn, K.-H. Highly fluorescent photochromic diarylethene with an excellent fatigue property. *J. Mater. Chem.* **2009**, *19*, 97−103.
(47) Kalayci, K.; Frisch, H.; Barner-Kowollik, C.; Truong, V. H. Wavelength-Dependent Stiffening of Hydrogel Matrices via Red-shifted [2 + 2] Photocycloadditions. *Adv. Funct. Mater.* **2020**, *30* (15), 1908171.
(48) Baghaffar, G. A.; Asiri, A. M. The Effects of Organic Additives on Photochromism. Part I: the Photochromic Performance of (E)-dicyclopropylmethylene-(2,5-dimethyl-3-furylethylidene)-succinic Anhydride and Ferrocene Containing Dye Doped in PMMA Polymer Film. *Pigm. Resin Technol.* **2008**, *37* (3), 145−150.
(49) Huang, W.; Abukhalil, P. M.; Khan, S. I.; Diaconescu, P. L. Group 3 Metal Stilbene Complexes: Synthesis, Reactivity, and Electronic Structure Studies. *Chem. Commun.* **2014**, *50* (40), 5221−5223.
(50) Khan, A.; Wang, L.; Yu, H.; Haroon, M.; Ullah, R. S.; Nazir, A.; Elshaarani, T.; Usman, M.; Fahad, S.; Haq, F. Research advances in the synthesis and applications of ferrocene-based electro and photo responsive materials. *Appl. Organomet. Chem.* **2018**, *32* (12), e4575.

https://doi.org/10.1021/acsapm.2c00090
ACS Appl. Polym. Mater. 2023, 5, 1−30

(51) Sun, S.; Liang, S.; Xu, W.-C.; Xu, G.; Wu, S. Photoresponsive polymers with multi-azobenzene groups. *Polym. Chem.* **2019**, *10*, 4389−4401.
(52) Zhang, Z.; Wang, W.; Jin, P.; Xue, J.; Sun, L.; Huang, J.; Zhang, J.; Tian, H. A building-block design for enhanced visible-light switching of diarylethenes. *Nat. Commun.* **2019**, *10*, 4232.
(53) Kamble, A. R.; Patel, C. M.; Murthy, Z. V. P. A review on the recent advances in mixed matrix membranes for gas separation processes. *Renew. Sust. Energy Rev.* **2021**, *145*, 111062.
(54) Qian, Q.; Asinger, P. A.; Lee, M. J.; Han, G.; Mizrahi Rodriguez, K.; Lin, S.; Benedetti, F. M.; Wu, A. X.; Chi, W. S.; Smith, Z. P. MOF-Based Membranes for Gas Separations. *Chem. Rev.* **2020**, *120* (16), 8161−8266.
(55) Zhang, Y.; Feng, X.; Yuan, S.; Zhou, J.; Wang, B. Challenges and recent advances in MOF-polymer composite membranes for gas separation. *Inorg. Chem. Front.* **2016**, *3* (7), 896−909.
(56) Aroon, M. A.; Ismail, A. F.; Matsuura, T.; Montazer-Rahmati, M. M. Performance Studies of Mixed Matrix Membranes for Gas Separation: A Review. *Sep. Purif. Technol.* **2010**, *75* (3), 229−242.
(57) Becker, D.; Konnertz, N.; Böhning, M.; Schmidt, J.; Thomas, A. Light-Switchable Polymers of Intrinsic Microporosity. *Chem. Mater.* **2016**, *28* (23), 8523−8529.
(58) Castellanos, S.; Goulet-Hanssens, A.; Zhao, F.; Dikhtiarenko, A.; Pustovarenko, A.; Hecht, S.; Gascon, J.; Kapteijn, F.; Bléger, D. Structural Effects in Visible-Light-Responsive Metal-Organic Frameworks Incorporating ortho-Fluoroazobenzenes. *Chem.—Eur. J.* **2016**, *22* (2), 746−752.
(59) Ludwanowski, S.; Skarsetz, O.; Creusen, G.; Hoenders, D.; Straub, P.; Walther, A. Wavelength-Gated Adaptation of Hydrogel Properties via Photo-Dynamic Multivalency in Associative Star Polymers. *Angew. Chem., Int. Ed.* **2021**, *60* (19), 4358−4367.
(60) Wandera, D.; Wickramasinghe, S. R.; Husson, S. M. Stimuli-responsive membranes. *J. Membr. Sci.* **2010**, *357* (1−2), 6−35.
(61) Ismail, A. F.; Khulbe, K. C.; Matsuura, T.Gas Separation Membranes. *Polymeric and Inorganic*; Springer, 2015.
(62) Kameda, M.; Sumaru, K.; Kanamori, T.; Shinbo, T. Photoresponsive Gas Permeability of Azobenzene-Functionalized Glassy Polymer Films. *J. Appl. Polym. Sci.* **2003**, *88* (8), 2068−2072.
(63) Bujak, K.; Nocon, K.; Jankowski, A.; Wolinska-Grabczyk, A.; Schab-Balcerzak, E.; Janeczek, H.; Konieczkowska, J. Azopolymers with Imide Structures as Light-switchable Membranes in Controlled Gas Separation. *Eur. Polym. J.* **2019**, *118*, 186−194.
(64) Nocoń-Szmajda, K.; Jankowski, A.; Wolińska-Grabczyk, A.; Konieczkowska, J. Guest-host and Functionalized Side-chain Azopolyimide Membranes for Controlled Gas Separation. *Polymer* **2021**, *229*, 124012.
(65) Chen, Z.; Xie, H.-Y.; Li, Y.-J.; Chen, G.-E; Xu, S.-J.; Xu, Z.-J. Smart Light Responsive Polypropylene Membrane Switching Reversibly between Hydrophobicity and Hydrophilicity for Oily Water Separation. *J. Membr. Sci.* **2021**, *638*, 119704.
(66) Chen, B.; Zhang, R.; Hou, Y.; Zhang, J.; Chen, S.; Han, Y.; Chen, X.; Hou, X. Light-responsive and Corrosion-resistant Gas Valve with Non-thermal Effective Liquid-gating Positional Flow Control. *Light Sci. Appl.* **2021**, *10*, 127.
(67) Batten, S. R.; Champness, N. R.; Chen, X.-M.; Garcia-Martinez, J.; Kitagawa, S.; Öhrström, L.; O'Keeffe, M.; Suh, M. P.; Reedijk, J. Coordination Polymers, Metal-Organic Frameworks and the Need for Terminology Guidelines. *CrystEngComm* **2012**, *14*, 3001−3004.
(68) Stock, N.; Biswas, S. Synthesis of Metal-Organic Frameworks (MOFs): Routes to Various MOF Topologies, Morphologies, and Composites. *Chem. Rev.* **2012**, *112* (2), 933−969.
(69) Lee, Y.; Kim, J.; Ahn, W. Synthesis of metal-organic frameworks: A mini review. *Korean J. Chem. Eng.* **2013**, *30* (9), 1667−1680.
(70) Hermann, D.; Emerich, H.; Lepski, R.; Schaniel, D.; Ruschewitz, U. Metal-Organic Frameworks as Hosts for Photochromic Guest Molecules. *Inorg. Chem.* **2013**, *52* (5), 2744−2749.
(71) Yanai, N.; Uemura, T.; Inoue, M.; Matsuda, R.; Fukushima, T.; Tsujimoto, M.; Isoda, S.; Kitagawa, S. Guest-to-Host Transmission of Structural Changes for Stimuli-Responsive Adsorption Property. *J. Am. Chem. Soc.* **2012**, *134* (10), 4501−4504.
(72) Hermann, A. D.; Schwartz, H. A.; Werker, M.; Schaniel, D.; Ruschewitz, U. Metal-Organic Frameworks as Hosts for Fluorinated Azobenzenes: A Path Towards Quantitative Photoswitching with Visible Light. *Chem.—Eur. J.* **2019**, *25*, 3606−3616.
(73) Jones, C. L.; Tansell, A. J.; Easun, T. L. The Lighter Side of MOFs: Structurally Photoresponsive Metal-Organic Frameworks. *J. Mater. Chem. A* **2016**, *4* (18), 6714−6723.
(74) Modrow, A.; Zargarani, D.; Herges, R.; Stock, N. The first porous MOF with photoswitchable linker molecules. *Dalton Trans.* **2011**, *40* (16), 4217−4222.
(75) Modrow, A.; Feyand, M.; Zargarani, D.; Herges, R.; Stock, N. Systematic Investigation of Porous Inorganic-Organic Hybrid Compounds with Photo-Switchable Properties. *Z. Anorg. Allg. Chem.* **2012**, *638*, 2138−2143.
(76) Wang, Z.; Tanabe, K. K.; Cohen, S. M. Accessing Postsynthetic Modification in a Series of Metal-Organic Frameworks and the Influence of Framework Topology on Reactivity. *Inorg. Chem.* **2009**, *48*, 296−306.
(77) Modrow, A.; Zargarani, D.; Herges, R.; Stock, N. Introducing a Photo-Switchable Azo-Functionality inside Cr-MIL-101-NH_2 by Covalent Post-Synthetic Modification. *Dalton Trans.* **2012**, *41* (28), 8690−8696.
(78) Healey, K.; Liang, W.; Southon, P. D.; Church, T. L.; D'Alessandro, D. M. Photoresponsive Spiropyran-Functionalised MOF- 808: Postsynthetic Incorporation and Light Dependent Gas Adsorption Properties. *J. Mater. Chem. A* **2016**, *4* (28), 10816−10819.
(79) Park, J.; Yuan, D.; Pham, K. T.; Li, J.-R.; Yakovenko, A.; Zhou, H.-C. Reversible Alteration of CO2 Adsorption upon Photochemical or Thermal Treatment in a Metal-Organic Framework. *J. Am. Chem. Soc.* **2012**, *134* (1), 99−102.
(80) Huang, R.; Hill, M. R.; Babarao, R.; Medhekar, N. V. CO_2 Adsorption in Azobenzene Functionalized Stimuli Responsive Metal-Organic Frameworks. *J. Phys. Chem. C* **2016**, *120* (30), 16658−16667.
(81) Yang, C.-T.; Kshirsagar, A. R.; Eddin, A. C.; Lin, L.-C.; Poloni, R. Tuning Gas Adsorption by Metal Node-Blocking in Photo-responsive Metal-Organic Frameworks. *Chem.—Eur. J.* **2018**, *24* (57), 15167−15172.
(82) Xie, M.; Prasetya, N.; Ladewig, B. P. Systematic Screening of DMOF-1 with NH_2, NO_2, Br and Azobenzene Functionalities for Elucidation of Carbon Dioxide and Nitrogen Separation Properties. *Inorg. Chem. Commun.* **2019**, *108*, 107512.
(83) Wang, Z.; Heinke, L.; Jelic, J.; Cakici, M.; Dommaschk, M.; Maurer, R. J.; Oberhofer, H.; Grosjean, S.; Herges, R.; Brase, S.; Reuter, K.; Woll, C. Photoswitching in Nanoporous, Crystalline Solids: An Experimental and Theoretical Study for Azobenzene Linkers Incorporated in MOFs. *Phys. Chem. Chem. Phys.* **2015**, *17*, 14582−14587.
(84) Patel, D. G.; Walton, I. M.; Cox, J. M.; Gleason, C. J.; Butzer, D. R.; Benedict, J. B. Photoresponsive Porous Materials: The Design and Synthesis of Photochromic Diarylethene-Based Linkers and a Metal-Organic Framework. *Chem. Commun.* **2014**, *50* (20), 2653−2656.
(85) Wang, Z.; Knebel, A.; Grosjean, S.; Wagner, D.; Bräse, S.; Wöll, C.; Caro, J.; Heinke, L. Tunable Molecular Separation by Nanoporous Membranes. *Natur. Commun.* **2016**, *7*, 13872.
(86) Coudert, F.-X. Responsive Metal-Organic Frameworks and Framework Materials: Under Pressure, Taking the Heat, in the Spotlight, with Friends. *Chem. Mater.* **2015**, *27* (6), 1905−1916.
(87) Prasetya, N.Development of Light-responsive Metal-organic Frameworks and Porous Materials and Their Application in Mixed Matrix Membranes for Gas Separation. Ph.D. Dissertation, Imperial College London, London, UK, 2019; https://spiral.imperial.ac.uk/handle/10044/1/73911 (accessed 2021-11-05).
(88) Prasetya, N.; Ladewig, B. P. New Azo-DMOF-1 MOF as a Photoresponsive Low-Energy CO_2 Adsorbent and Its Exceptional CO_2/N_2 Separation Performance in Mixed Matrix Membranes. *ACS Appl. Mater. Interfaces* **2018**, *10* (40), 34291−34301.

https://doi.org/10.1021/acsapm.2c00090
ACS Appl. Polym. Mater. 2023, 5, 1−30

(89) Prasetya, N.; Donose, B. C.; Ladewig, B. P. A New and Highly Robust Light-responsive Azo-UiO-66 for Highly Selective and Low Energy Post-combustion CO_2 Capture and its Application in a Mixed-Matrix Membrane for CO_2/N_2 Separation. *J. Mater. Chem. A* **2018**, *6* (34), 16390−16402.
(90) Prasetya, N.; Ladewig, B. P. An Insight on the Effect of Azobenzene Functionalities Studied in UiO-66 Framework for Low Energy CO_2 Capture and CO_2/N_2 Membrane Separation. *J. Mater. Chem. A* **2019**, *7*, 15164−15172.
(91) Prasetya, N.; Teck, A. A.; Ladewig, B. P. Matrimid-JUC-62 and Matrimid-PCN-250 Mixed Matrix Membranes Displaying Light-Responsive Gas Separation and Beneficial Ageing Characteristics for CO_2/N_2 Separation. *Sci. Rep.* **2018**, *8*, 2944.
(92) Xin, Q.; Cao, X.; Huang, D.; Li, S.; Zhang, X.; Xuan, G.; Wei, M.; Zhang, L.; Ding, X.; Zhang, Y. Smart Light-responsive Hierarchical Metal-Organic Frameworks Constructed Mixed-Matrix Membranes for Efficient Gas Separation. *Green Chem. Eng.* **2022**, *3*, 71−82.
(93) Luo, F.; Fan, C. B.; Luo, M. B.; Wu, X. L.; Zhu, Y.; Pu, S. Z.; Xu, W.; Guo, G. Photoswitching CO_2 Capture and Release in a Photochromic Diarylethene Metal-Organic Framework. *Angew. Chem., Int. Ed.* **2014**, *53* (35), 9298−9301.
(94) Nikolayenko, V. I.; Herbert, S. A.; Barbour, L. J. Reversible Structural Switching of a Metal-Organic Framework by Photo-Irradiation. *Chem. Commun.* **2017**, *53* (81), 11142−11145.
(95) Zhang, S.; Ma, J.; Zhang, X.; Duan, E.; Cheng, P. Assembly of Metal-Organic Frameworks Based on 3, 3, 5, 5-Azobenzene-tetracarboxylic Acid: Photoluminescences, Magnetic Properties, and Gas Separations. *Inorg. Chem.* **2015**, *54* (2), 586−595.
(96) Dang, L.-L.; Zhang, X.-J.; Zhang, l.; Li, J.-K.; Luo, F.; Feng, X.-F. Photo-responsive azo-MOF Exhibiting High Selectivity for CO_2 and Xylene Isomers. *J. Coord. Chem.* **2016**, *69* (7), 1179−1187.
(97) Fan, C. B.; Liu, Z. Q.; Gong, L. L.; Zheng, A. M.; Zhang, L.; Yan, C. S.; Wu, H. Q.; Feng, X. F.; Luo, F. Photoswitching Adsorption Selectivity in a Diarylethene-Azobenzene MOF. *Chem. Commun.* **2017**, *53* (4), 763−766.
(98) Prasetya, N.; Ladewig, B. P. Dynamic Photo-Switching in Light-Responsive JUC-62 for CO_2 Capture. *Sci. Rep.* **2017**, *7*, 13355.
(99) Li, S.; Prasetya, N.; Ladewig, B. P. Investigation of Azo-COP-2 as a Photoresponsive Low-Energy CO_2 Adsorbent and Porous Filler in Mixed Matrix Membranes for CO_2/N_2 Separation. *Ind. Eng. Chem. Res.* **2019**, *58* (23), 9959−9969.
(100) Alrayyes, A. U.; Hu, Y.; Tabor, R. F.; Wang, H.; Saito, K. Photo-Switchable Membranes Constructed from Graphene oxide/star-PDMS Nanocomposites for Gas Permeation Control. *J. Mater. Chem. A* **2021**, *9* (37), 21167−21174.
(101) Haldar, R.; Wöll, C. Hierarchical Assemblies of Molecular Frameworks - MOF-on-MOF Epitaxial Heterostructures. *Nano Res.* **2021**, *14*, 355−368.
(102) Fu, W.-Q.; Liu, M.; Gu, Z.-G.; Chen, S.-M.; Zhang, J. Liquid Phase Epitaxial Growth and Optical Properties of Photochromic Guest-Encapsulated MOF Thin Film. *Cryst. Growth Des.* **2016**, *16* (9), 5487−5492.
(103) Heinke, L.; Cakici, M.; Dommaschk, M.; Grosjean, S.; Herges, R.; Bräse, S.; Wöll, C. Photoswitching in Two-Component Surface-Mounted Metal-Organic Frameworks: Optically Triggered Release from a Molecular Container. *ACS Nano* **2014**, *8* (2), 1463−1467.
(104) Knebel, A.; Sundermann, L.; Mohmeyer, A.; Strauß, I.; Friebe, S.; Behrens, P.; Caro, J. Azobenzene Guest Molecules as Light-Switchable CO_2 Valves in an Ultrathin UiO-67 Membrane. *Chem. Mater.* **2017**, *29* (7), 3111−3117.
(105) Müller, K.; Wadhwa, J.; Singh Malhi, J.; Schöttner, L.; Welle, A.; Schwartz, H.; Hermann, D.; Ruschewitz, U.; Heinke, L. Photoswitchable Nanoporous Films by Loading Azobenzene in Metal-Organic Frameworks of Type HKUST-1. *Chem. Commun.* **2017**, *53* (57), 8070−8073.
(106) Yu, X.; Wang, Z.; Buchholz, M.; Füllgrabe, N.; Grosjean, S.; Bebensee, F.; Bräse, S.; Wöll, C.; Heinke, L. *Cis*-to-*trans* Isomerization of Azobenzene Investigated by Using Thin Films of Metal-Organic Frameworks. *Phys. Chem. Chem. Phys.* **2015**, *17* (35), 22721−22725.
(107) Muller, K.; Knebel, A.; Zhao, F.; Bleger, D.; Caro, J.; Heinke, L. Switching Thin Films of Azobenzene-Containing Metal-Organic Frameworks with Visible Light. *Chem.—Eur. J.* **2017**, *23* (23), 5434−5438.
(108) Jiang, Y.; Heinke, L. Photoswitchable Metal-Organic Framework Thin Films: From Spectroscopy to Remote-Controllable Membrane Separation and Switchable Conduction. *Langmuir* **2021**, *37* (1), 2−15.
(109) Weh, K.; Noack, M.; Hoffmann, K.; Schröder, K.-P.; Caro, J. Change of Gas Permeation by Photoinduced Switching of Zeolite-Azobenzene Membranes of Type MFI and FAU. *Microporous Mesoporous Mater.* **2002**, *54* (1−2), 15−26.
(110) Soukup, K.; Schneider, P.; Šolcová, O. Comparison of Wicke-Kallenbach and Graham's Diffusion Cells for Obtaining Transport Characteristics of Porous Solids. *Chem. Eng. Sci.* **2008**, *63* (4), 1003−1011.
(111) Sridhar, S.; Bee, S.; Bhargava, S. K. Membrane-based Gas Separation: Principle, Applications and Future Potential. *J. Membr. Sci.* **2014**, *77*−*87*, 1−25.
(112) Šolcová, O.Chemical Engineering Aspects of Gas Transport in Porous Solids. Ph.D. Dissertation, Academy of Sciences of the Czech Republic, Praha, Czech Republic, 2011; https://www.avcr.cz/export/sites/avcr.cz/cs/pro-verejnost/.content/soubory/dsc-teze/Solcova_DSc-teze.pdf (accessed 2021-11-06).
(113) Liu, C.; Jiang, Y.; Zhou, C.; Caro, J.; Huang, A. Photo-Switchable Smart Metal-Organic Frameworks Membranes with Tunable and Enhanced Molecule Sieving Performance. *J. Mater. Chem. A* **2018**, *6* (48), 24949−24955.

https://doi.org/10.1021/acsapm.2c00090
ACS Appl. Polym. Mater. 2023, 5, 1−30